# Interfacial bonding and corrosion inhibition of 2-mercaptobenzimidazole organic films formed on copper surfaces under electrochemical control in acidic chloride solution

Vishant Garg, Sandrine Zanna, Antoine Seyeux, Frédéric Wiame, Vincent Maurice, Philippe Marcus

▶ **To cite this version:**

Vishant Garg, Sandrine Zanna, Antoine Seyeux, Frédéric Wiame, Vincent Maurice, et al.. Interfacial bonding and corrosion inhibition of 2-mercaptobenzimidazole organic films formed on copper surfaces under electrochemical control in acidic chloride solution. Electrochimica Acta, 2024, 484, pp.144114. 10.1016/j.electacta.2024.144114 . hal-04505820

**HAL Id: hal-04505820**
**https://hal.science/hal-04505820**

Submitted on 15 Mar 2024

**HAL** is a multi-disciplinary open access archive for the deposit and dissemination of scientific research documents, whether they are published or not. The documents may come from teaching and research institutions in France or abroad, or from public or private research centers.

L'archive ouverte pluridisciplinaire **HAL**, est destinée au dépôt et à la diffusion de documents scientifiques de niveau recherche, publiés ou non, émanant des établissements d'enseignement et de recherche français ou étrangers, des laboratoires publics ou privés.

Distributed under a Creative Commons Attribution 4.0 International License

Author preprint published in *Electrochimica Acta*
https://doi.org/10.1016/j.electacta.2024.144114

# Interfacial bonding and corrosion inhibition of 2-mercaptobenzimidazole organic films formed on copper surfaces under electrochemical control in acidic chloride solution

Vishant Garg, Sandrine Zanna, Antoine Seyeux,

Frédéric Wiame, Vincent Maurice[1], Philippe Marcus[2]

*PSL University, CNRS – Chimie ParisTech, Institut de Recherche de Chimie Paris,*

*Physical Chemistry of Surfaces Research Group,*

*11 rue Pierre et Marie Curie, 75005 Paris, France.*

[1]Corresponding author for the work: vincent.maurice@chimieparistech.psl.eu

[2]Corresponding author for the work: philippe.marcus@chimieparistech.psl.eu

## Abstract

The interfacial bonding and the layered structure of 2-mercaptobenzimidazole (2-MBI) organic films adsorbed on electrochemically controlled copper surfaces and their corrosion inhibition effects in acidic chloride aqueous solution were investigated using an integrated approach of electrochemical methods and advanced surface analyses by X-ray photoelectron spectroscopy and time-of-flight secondary ion mass spectrometry. It is shown that organic films formed on the copper surfaces are bi-layered with a chemisorbed inner layer and a physisorbed outer layer. In the chemisorbed inner layer, 2-MBI is bonded primarily by its nitrogen atoms with metallic and oxidized copper surfaces. Sulphur atoms are also involved in the bonding mechanism when metallic copper is directly accessible to the 2-MBI molecules. The initial presence of native copper oxides at the interface promotes the formation of Cu(I)-2-MBI metal-organic complexes in the chemisorbed inner layer using cathodic reduction to dissociate the oxide. Metal-organic complexes also form upon anodic polarisation due to Cu(I) ions generated by oxidation of the copper metal. 2-MBI effectively inhibits copper anodic dissolution in varying degrees, between 84% and 93%, depending on the pre-treatment used for the formation of the organic bi-layers. An enhanced protection of the substrate is obtained by adsorbing the 2-MBI inhibitor on an initially oxide-free surface, which is achieved by cathodic pre-treatment in absence of the inhibitor followed by 1 hour exposure to the inhibitor.

## Keywords

Copper, Corrosion Inhibitor, 2-mercaptobenzimidazole, Electrochemistry, Surface Analysis, XPS, ToF-SIMS.

## Introduction

Copper, like most metals, is susceptible to corrosion despite its high nobility among other metals. Since copper has wide ranging applications from its use in pipes for plumbing systems, electrical components, heat exchangers, construction materials, industrial machinery, and even cannisters for the storage of nuclear waste, it poses a serious issue that could have major implications. Although copper is protected in neutral and alkaline environments due to the formation of a passive oxide film that covers and protects the surface [1–6], it is highly vulnerable to attack in acidic environments where this oxide film readily dissolves thus leaving the metal substrate exposed to corrosive agents [7–13]. Additionally, aggressive ions such as sulphates, nitrates, and halides can result in degradation of the metal even in neutral and alkaline conditions [14–16]. Therefore, it is imperative to investigate techniques which could protect copper from degradation in acidic environments and other corrosive environments. One such technique is the application of inhibitors [17–20], which are chemical compounds that suppress reactions from occurring on a metal surface by forming an isolating barrier on the surface, thus inhibiting corrosion of the metal.

2-mercaptobenzimidazole (2-MBI), with the chemical formula $C_7H_6N_2S$, is often used as a corrosion inhibitor to protect metals such as copper, copper alloys, zinc, stainless steels, and aluminium alloys [21–31]. The 2-MBI molecule consists of a benzene ring ($C_6H_4$) bonded to two nitrogen atoms, forming another cycle with a carbon atom attached between them. This carbon atom is further bonded to an exocyclic sulphur atom, the bonding of which depends on the environment thus dictating the dominant conformer of the molecule [32]. The various conformers of the 2-MBI molecule – thione, thiol, and thiolate are depicted in the models shown in Figure 1. In the work of Ansar et al. [33], it was determined that 2-MBI exists predominantly in the thione form in the solid state and in polar solvents. In strongly alkaline solutions, 2-MBI ionizes to its thiolate conformer. The changes in the dominant conformer of 2-MBI occur due to the pKa of the molecule, which is 10.4 [33,34], thus determining the stability of the molecule based on the pH of the environment and the other species present in that environment.

Several researchers have investigated the use of 2-MBI as an effective corrosion inhibitor for copper, both experimentally and theoretically, mostly due to the presence of S and N heteroatoms [21–24,35–39]. These heteroatoms, which act as active sites, allow the molecule

to bond with the metal surface and form a dense and protective film [21,35]. The aforementioned works have explored various aspects of the 2-MBI adsorption and inhibition on copper. The adsorption of 2-MBI from the vapour phase on clean, 2-D oxide, and 3-D oxide-covered copper surfaces was investigated in the works of Wu et al. [21,22]. It was found that 2-MBI adsorbed on metallic copper surfaces by its sulphur and both nitrogen atoms with the molecule lying flat on copper. On oxidized surfaces, the bonding occurred via the sulphur atom and only one nitrogen atom with a tilted geometry on the surface. These bonding mechanisms between the 2-MBI molecule and copper were also suggested by Density Functional Theory calculations in the work of Chiter et al. [37,38], thus exhibiting unanimity between theoretical and experimental work. Additionally, these findings also corroborated the results of Finsgar et al. [35], who found that 2-MBI bonds to the oxidized copper by its S and N atoms, thus resulting in a tilted position on the surface. They also demonstrated that 2-MBI is indeed an effective inhibitor against corrosion in a 3% NaCl solution [24].

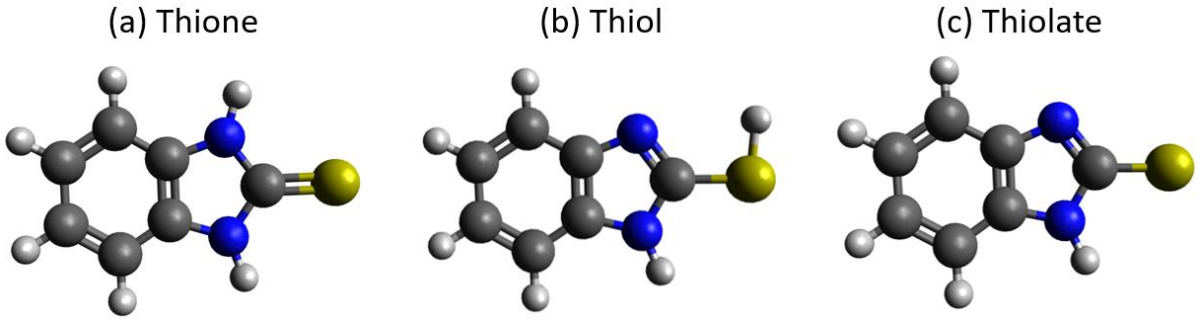


*Figure 1: Models illustrating the various conformers of the 2-MBI molecule ($C_7H_6N_2S$): (a) thione form, (b) thiol form, and (c) thiolate form. The yellow atoms represent the sulphur, the blue atoms represent the nitrogen, the grey atoms represent the carbon, and the white atoms represent the hydrogen atoms in the molecule.*

The inhibition of intergranular corrosion by 2-MBI on copper using in-situ electrochemical scanning tunnelling microscopy was evaluated by Sharma et al. [23]. In their work, it was established that 2-MBI protects copper, although imperfectly, from corrosion. They also suggested that the formation of Cu(I)-MBI reaction products may be the reason for protection against dissolution in an acidic environment. This formation of the Cu(I)-MBI complex film and its corrosion protection properties has also been proposed by others [34,40,41].

The formation of the Cu(I)-MBI complexes occurs due to the dissolution of copper oxides in acidic environment which provides a steady supply of $Cu^+$ ions for the complexes, as proposed by Chadwick and Hashemi [40]. On prolonged exposure to the acidic solution, they observed

that the thickness of the complex films increases due to additional $Cu^{+}$ ions generated by the anodic dissolution of the copper metal, thus relating the thickness of the complex film to the pH of the solution. On the other hand, Xue et al. [41] reported that the complex films formed between Cu and 2-MBI are different depending on the oxidation state of copper. When 2-MBI reacts with copper oxides, it results in the formation of Cu(I)-2-MBI complex film with the C=S bond intact in the 2-MBI molecule, whereas when the molecule interacts with metallic copper, the complex film formed is mainly $Cu^{+}MBI^{-}$ or $Cu_2^{+}MBI^{2-}$ with the C=S bond being split in the 2-MBI molecule. Both complex films are suggested to be protective against corrosion, although the latter complex film is reported to be less defective and therefore more protective.

Despite these numerous works, there remains some ambiguity on the formation and protective capabilities of the 2-MBI film formed on metallic copper and oxidized copper surfaces, especially in the presence of aggressive species such as chloride ions which can compete with the inhibitor molecules to interact with the metal. Furthermore, it is essential to understand how the presence of oxides plays a role on the inhibitive properties of the barrier layer formed. Though the above-mentioned works have addressed some of the points individually, we know that in a real-world perspective the combined effect of each element may distort and alter the behaviour of the inhibitor for corrosion protection of copper.

In the present work, we optimise the conditions of formation of the 2-MBI organic film by electrochemical control of the copper surface in an acidic chloride media and investigate the resulting bonding mechanisms between the inhibitor and copper. We also evaluate the corrosion inhibition offered to the substrate by the different organic layers formed on each surface, and the effect of anodic polarization on the stability of the 2-MBI organic layer. The desired interfaces were formed by cathodic pre-treatment of the surfaces either in presence or absence of the inhibitor in the solution. Advanced surface analysis, using X-ray photoelectron spectroscopy (XPS) and time-of-flight secondary ion mass spectrometry (ToF-SIMS), was performed to evaluate the bonding mechanisms and the role of the oxides on the formation of the 2-MBI organic layer. Cyclic Voltammetry (CV) was applied to determine the protective capabilities of the organic layers against corrosion. ToF-SIMS and XPS surface analyses were performed to characterize the inhibited interfaces and their alterations after

polarization and to examine whether the protection offered to the copper metal substrate by the 2-MBI films was effective.

## Experimental

The samples used for experimental analysis were polycrystalline copper samples obtained from high purity cast electrolytic tough pitch copper with minimal contamination [42], as in previous works [43–45]. The samples were mechanically polished using silicon carbide papers up to 4000 grit to obtain a flat surface, followed by diamond pastes down to 0.25 µm to obtain a mirror finish surface. They were rinsed with ethanol and ultra-pure water (resistivity > 18.2 MΩ) after each polishing step and were ultrasonically cleaned for 5 minutes in successive baths of acetone, ethanol, and ultra-pure water after the final polishing step. Electrochemical polishing was performed on each sample following mechanical polishing in a 60% solution of $H_3PO_4$. A constant voltage of 1.4 V was applied for 4 minutes using a copper plate as the counter electrode. This step removes the cold-worked layer on the surface of the sample along with contaminants present on the surface [46]. The samples were finally rinsed with a 10% $H_3PO_4$ solution, followed by ultra-pure water, and then dried using nitrogen.

The electrochemical tests were performed in cells made of polychlorotrifluoroethylene, more commonly known as Kel-F, equipped with a counter electrode and a pseudo-reference electrode made of platinum. The volume of the electrolyte in the Kel-F cell was approximately 350 – 400 µl. The cells were cleaned thoroughly prior to each experiment using a 2:1 volumetric solution of $H_2SO_4$ and $H_2O_2$, followed by concentrated $HNO_3$, and finally rinsed in boiling ultra-pure water several times. The pseudo reference electrode was calibrated before each experiment to ensure correct measurement of the potentials. The platinum electrode was calibrated to be +0.75 V vs SHE. The working electrode area, delimited by an O-ring, was 0.16 $cm^2$. A PicoStat bi-potentiostat and the Picoscan software from Agilent Technologies were used for performing the experiments. The electrolytes used were a 10 mM HCl reference aqueous solution of pH 2.3 ± 0.1 (solution without inhibitor), and a 10 mM HCl + 1 mM 2-MBI aqueous solution of pH 2.4 ± 0.1 (solution with inhibitor). All chemicals used were of analytical grade and were supplied by Sigma Aldrich and VWR chemicals.

Reduction of the native oxides of copper were carried out by cathodic pre-treatment of the substrate surfaces. The samples were immersed in the Kel-F cells at the open circuit potential

(OCP), following which the potential was swept cathodically to the onset of hydrogen evolution at – 0.05 V vs SHE, with a scan rate of 20 mV/s, and then back up to the value of + 0.10 V vs SHE, the potential at which the measured current was 0 µA/cm². This was repeated 2 times to ensure maximum reduction of the air formed native oxides present on the surface. For surfaces pre-treated in the reference HCl solution (absence of inhibitor), the solution was replaced after cathodic pre-treatment by removing approximately 3/4$^{th}$ of the solution using a pipette and adding the inhibitor containing solution to the cell while the electrodes were still immersed and connected to the potentiostat. This was repeated 7 times to replace the inhibitor-free solution with the inhibitor containing solution. For the surfaces pre-treated in the presence of inhibitor, no change in solution was carried out. The anodic dissolution tests were performed using cyclic voltammetry, by sweeping the potential up to the anodic apex at + 0.37 V vs SHE or higher, followed by reverse sweeping to – 0.05 V vs SHE, and back to the initial potential of + 0.10 V vs SHE. The experiments were repeated 3 times each to ensure reproducibility of the results.

Surface analysis using XPS and ToF-SIMS were performed on the surfaces after cathodic pre-treatment and deposition of the 2-MBI molecule on the surface (reduced state at + 0.10 V vs SHE), and after sweeping the potential to the anodic apex in the polarized state (anodic state at + 0.37 V vs SHE). Once the desired state of the surface was achieved, the cell was disconnected, the samples were rinsed with ultra-pure water, dried using nitrogen, and transferred to the ultra-high vacuum (UHV) chamber for analysis immediately.

XPS analysis was performed with a Thermo Electron Escalab 250 Xi spectrometer, using a monochromated Al Kα X- ray source (hv = 1486.6 eV), operating at a base pressure less than $10^{-10}$ mbar. An X-ray spot size of 900 µm in diameter was used, and the take-off angle of the collected photoelectrons was 90°. The survey spectra were recorded with a pass energy of 100 eV at a step size of 1 eV, while the high-resolution spectra of the C 1s, O 1s, N 1s, S 2p, Cl 2p, Cu 2p core levels and Cu LMM Auger transition were recorded with a pass energy of 20 eV at a step size of 0.1 eV. Decomposition of the spectra was performed with Avantage, the Thermo Fischer scientific software, using an iterative Shirley-type background. The binding energies were referred to the Fermi level of the sample. The photoionization cross-section values at 1486.6 eV were taken from the Scofield database [47], the inelastic mean free paths

were calculated using the TPP-2M formula [48], and the transmission function of the analyser was provided by Thermo Fischer.

ToF-SIMS analysis was performed using a ToF-SIMS 5 spectrometer (IonTof – Münster Germany), operating at a base pressure of 5 x $10^{-9}$ mbar. Analysis was done in high current bunched mode to obtain a high mass resolution. Negative depth profiles are performed by sequentially analysing the surface (25 keV $Bi^+$ primary ions with a target current of 1.2 pA over an area of 100 x 100 µm²) and sputtering the surface (0.5 keV $Cs^+$ ions with a target current of 20 nA over an area of 500 x 500 µm²). Both ion beams were at a 45° incidence angle to the surface of the sample and were well-aligned to ensure analysis at the centre of the sputtered crater. Data acquisition and post-processing analysis were performed using the SurfaceLab software v7.2. Three measurements were recorded on each sample from different regions to ensure reproducibility.

## Results and Discussion

### Reduction of native oxides by cathodic pre-treatment of the interface

The cathodic pre-treatment curves obtained for the reduction of the air formed native oxides in the absence and presence of 2-MBI in the HCl solution are shown in Figure 2. The cathodic charge density of the three cycles determined by integrating the cathodic current density with respect to time are presented in Table 1.

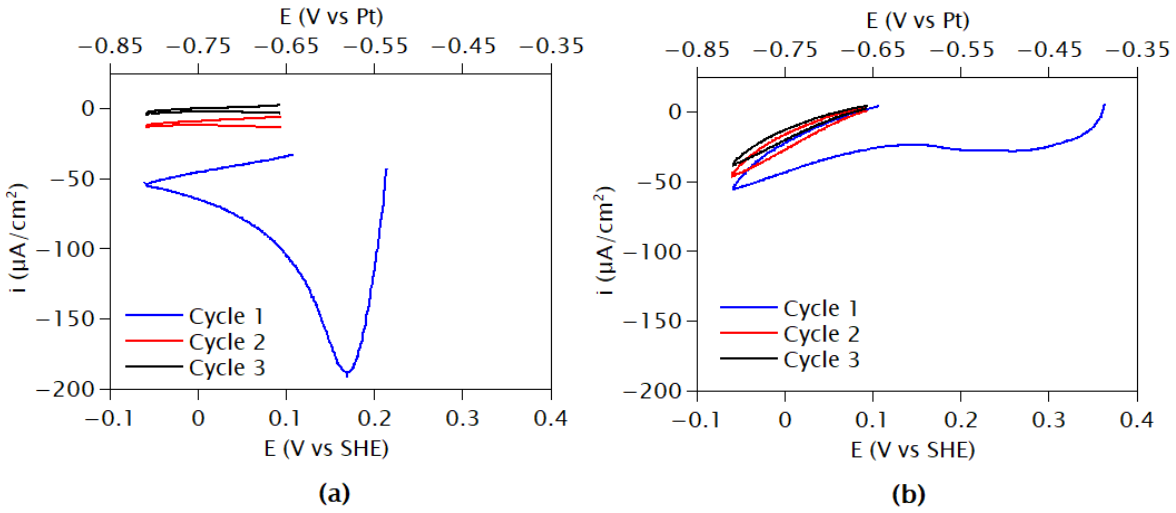


*Figure 2: Cathodic pre-treatment CVs of copper obtained in (a) 10 mM HCl reference solution, and (b) 10 mM HCl solution with 1 mM 2-MBI (scan rate of 20 mV/s).*

For the first cycle of cathodic pre-treatment in absence of 2-MBI (Figure 2a), the open circuit potential (OCP) measured at immersion was 0.21 V vs SHE. The reduction peak occurs at a potential of 0.18 V vs SHE with a significantly large cathodic charge density measured (1698 ± 38 μC/cm² from Table 1). The equivalent thickness of oxide reduced during this cycle, estimated using Faraday's Law [49], was 2.10 ± 0.01 nm, where the molar volume of $Cu_2O$ was taken as 23.9 $cm^3$/mol and the number of electrons exchanged per $Cu_2O$ molecule was 2. Additionally, in this case, the dissolution of the native oxides also occurs at OCP, prior to the first cycle of pre-treatment, due to the low pH of the electrolyte. However, the quantity of oxides dissolved at OCP cannot be quantified.

The first cycle of pre-treatment in presence of 2-MBI (Figure 2b) exhibits a stark difference with the previous case. The OCP measured at immersion was 0.34 V vs SHE, significantly higher than in absence of 2-MBI with an increase of +0.13 V. This indicates that 2-MBI adsorbs on the surface immediately on immersion in the 2-MBI containing solution and before the start of

the cathodic pre-treatment cycles. We also observe the absence of a prominent reduction peak, and the measured charge density is lower by a factor of approximately 2.3 times (Table 1). This is most likely due to 2-MBI adsorbed on the substrate surface, either in the form of an organic layer or in the form of metal-organic complexes due to a conversion reaction, which prevents the reduction of native oxides. Since there is no reduction peak, we did not estimate the thickness of oxides reduced, if any oxides were reduced at all. Since the inhibitor is likely to restrict the access of the oxide layer from the electrolyte, we cannot confirm the dissolution of oxides at OCP due to the low pH of the electrolyte.

*Table 1: Cathodic charge densities in μC/cm² determined from the three cycles of cathodic pre-treatment of copper in 10 mM HCl solution (without inhibitor), and in 1 mM 2-MBI + 10 mM HCl solution (with inhibitor), by integrating the current density measured with time.*

| Cycle | Cathodic charge densities (μC/cm²) | |
|---|---|---|
| | Pre-treatment without 2-MBI | Pre-treatment with 2-MBI |
| 1 | 1698 ± 38 | 751 ± 15 |
| 2 | 165 ± 9 | 284 ± 14 |
| 3 | 32 ± 5 | 211 ± 1 |

The next two cycles of pre-treatment in the absence of 2-MBI (Figure 2a) shows progressively lower cathodic charge densities measured (Table 1), indicating a nearly complete reduction of the native oxides on this substrate. The curves obtained for the second and third cycles of pre-treatment in the presence of 2-MBI (Figure 2b) also measured very low charge densities, although slightly higher than that of pre-treatment in absence of 2-MBI. However, no reduction peak was observed, similar to the first cycle, confirming that the reduction of native oxides is blocked, possibly due to an interaction between the organic molecules and the copper oxides present, as suggested by others [40,41].

## Surface analysis after adsorption of 2-MBI

To evaluate the surface state after cathodic pre-treatment, surface analysis was carried out on copper samples pre-treated in absence of 2-MBI followed by 1 hour exposure to 2-MBI, hereafter labelled (a), and on samples pre-treated in presence of 2-MBI, hereafter labelled (b). In the former pre-treatment method (without inhibitor), the inhibitor containing solution was introduced after the pre-treatment cycles as specified earlier in the experimental section.

The elemental ToF-SIMS depth profiles are presented in Figure 3, with the intensity in counts, plotted in logarithmic scale to enhance the low intensity signals, *vs.* sputtering time in seconds. The selected ions are $Cu^-$, $CuO^-$, $O^-$, and $^{37}Cl^-$, characteristic of the copper substrate, copper oxide, overall oxygen, and overall chlorine, respectively. The $C_7H_4N_2S^-$ ions were selected as characteristic of the 2-MBI molecule, and the $CuC_6H_4NS^-$, $CuS^-$, and $CuN_2^-$ ions as representative of Cu interaction with the 2-MBI molecule in its entirety and its respective fragments. The difference in the number of carbon atoms between the ions selected as representative of the 2-MBI molecule and representative of Cu interaction with 2-MBI is due to the different ionization yields of the molecule resulting in varying signatures obtained for each species. The limits of each layer were defined by the maximum intensity of the corresponding ions with an uncertainty of 5%.

It is observed that for the sample pre-treated in absence of 2-MBI followed by 1 hour exposure to 2-MBI, Figure 3a, the maximum intensity of the $Cu^-$ ion profile, which indicates the metal-oxide interface, corresponds to 120 seconds of sputtering. We also observe that the maximum intensity of the $CuO^-$ ion profile is at 20 seconds of sputtering, indicating that the oxide interface is of approximately 100 seconds of sputtering time. Similarly, both the $CuS^-$ ion profile and the $CuN_2^-$ ion profile peak at 20 seconds of sputtering, indicating that the interaction between copper and the molecule occurs with both the nitrogen and sulphur atoms. This is in contrast to that observed for 2-MBT adsorption on copper in an acidic chloride environment, where the sulphur was found at a greater sputtering time than the nitrogen of the molecule [43].

In the present case, the copper oxide profile peaks at the same sputtering time as the copper-sulphur and copper-nitrogen interaction and follows a similar decreasing profile until 120 seconds of sputtering. This indicates that the oxides subsist at the interface as islands along with the Cu-S and Cu-N interactions, as seen in previous works on 2-MBT adsorption on copper surfaces [43–45]. This feature is corroborated with the peak of the $O^-$ ion profile, also occurring at 20 seconds of sputtering.

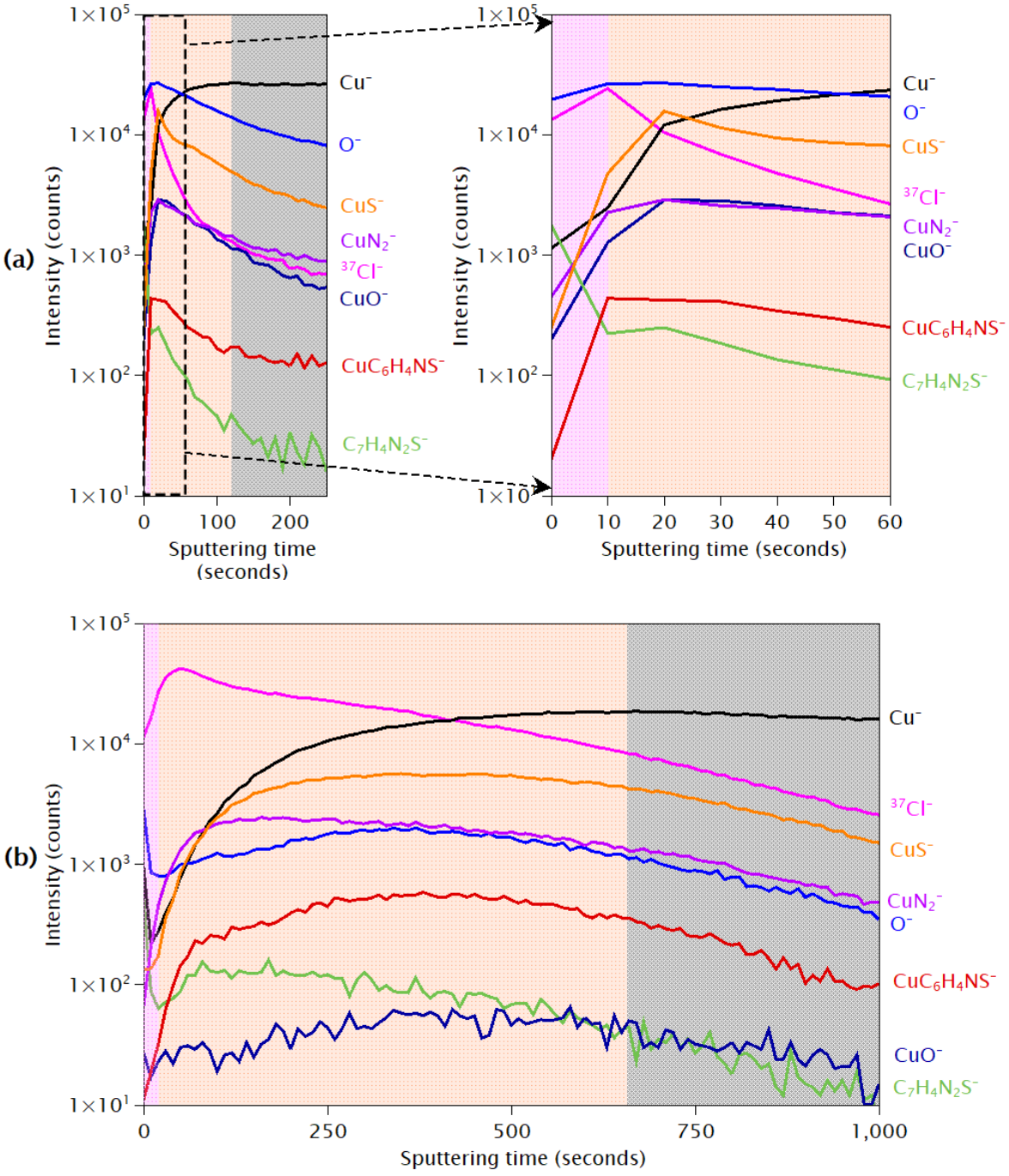


*Figure 3: ToF-SIMS depth profiles obtained for 2-MBI films formed on copper surfaces at the reduced state in 10 mM HCl solution after cathodic pre-treatment (a) in the absence of 2-MBI followed by 1 hour exposure to 2-MBI, and (b) in the presence of 2-MBI.*

The ion profile of $C_7H_4N_2S^-$, corresponding to the 2-MBI molecule, exhibits a sharp decrease in intensity from the initial top-most surface to 10 seconds of sputtering, followed by a slower decrease thereafter. This suggests multi-layers of the 2-MBI film physisorbed on the surface, also observed in previous work with 2-MBT organic inhibitor [43–45]. The $CuC_6H_4NS^-$ ion

profile, representative of Cu bonding with 2-MBI molecule, exhibits an increase in intensity up to 10 seconds, followed by a plateau until 30 seconds of sputtering. The initial low intensity is consistent with the absence of Cu-2-MBI bonding near the top-most surface. The following increase and the subsequent plateau are indicative of an inner chemisorbed layer, in which the 2-MBI molecules bond to the copper substrate. After 30 seconds there is a gradual decrease in intensity up to 120 seconds of sputtering, where the Cu substrate is reached.

The $^{37}Cl^-$ ion profile peaks near the surface and decreases sharply immediately after the peak. This suggests that the chlorine is mostly present in the outer organic layer and its interaction is rather limited with the metal substrate due to the inner organic layer acting as a barrier between the substrate and the chlorine ions, thus indicating effectiveness of the 2-MBI barrier layer formed by this pre-treatment method.

In Figure 3b, pre-treatment in presence of 2-MBI, it is observed that the metal oxide interface is at 657 seconds of sputtering time (maximum intensity of the $Cu^-$ ion profile). The time taken to reach the interface for this sample is a drastic increase as compared to that for the pre-treatment shown in Figure 3a. This increase in sputtering time is indicative of the formation of much thicker organic layers on the sample. We also observe an increased roughness of the inhibited interface, attested by the progressive increase of the $Cu^-$ signal. The $CuN_2^-$ ion profile peaks at 180 seconds of sputtering, while the $CuS^-$ ion profile peaks at 360 seconds, suggesting mostly sulphur interaction with the substrate, unlike the previous case (Figure 3a) where both ion profiles peaked at the same sputtering time.

Next, the $CuO^-$ ion profile does not exhibit a definite peak, rather a slightly curved profile centered around 400 seconds of sputtering. This is in contrast with the pre-treatment in absence of 2-MBI (Figure 3a), where a well-defined peak was observed for the $CuO^-$ ion profile. Additionally, in this case (Figure 3b), the intensity of the $CuO^-$ ion profile is extremely low throughout the sputtering duration. On the other hand, the $O^-$ ion profile exhibits an intensity decrease for the first 10 seconds of sputtering, followed by a similar curve centered around 360 seconds. This suggests that, in this case (Figure 3b), there are much smaller traces of copper oxides remaining at the interface that in the previous case (Figure 3a).

The $C_7H_4N_2S^-$ ion profile (Figure 3b) exhibits a decrease in intensity for the first 20 seconds of sputtering, similar to the previous case (Figure 3a), suggesting the presence of an outer layer

of the organic film. However, a similar decreasing trend is observed in this case for the $Cu^-$ and $O^-$ ion profiles for the first 20 seconds of sputtering. This could be possibly due to complexes formed by an interaction with copper oxides and the 2-MBI molecule, which would be deposited on the surface, as proposed by others [40,41]. This phenomenon of the initial decrease in the intensity of the depth profiles corresponding to the molecule and copper has also been observed in previous work of 2-MBT adsorption on copper in neutral and alkaline media signifying the presence of complexes [44,45].

The $CuC_6H_4NS^-$ ion profile (Figure 3b) exhibits a sharp increase in intensity up to 60 seconds, followed by a slower and gradual increase in intensity up until 400 seconds of sputtering, confirming the presence of a thicker barrier layer on this sample. The ion profile shape is also in agreement with the interaction between copper and the molecule fragments seen with the $CuN_2^-$ and $CuS^-$ ion profiles. This would likely correspond to the Cu-2-MBI conversion layer formed by a reaction between the oxides and 2-MBI during cathodic pre-treatment. After 400 seconds, a gradual decrease in intensity is observed for the $CuC_6H_4NS^-$ ion profile till the Cu substrate is reached, similar to the sample pre-treated in absence of 2-MBI (Figure 3a) in terms of profile shape.

The $^{37}Cl^-$ ion profile exhibits its maximum intensity near the surface, like in the previous case. Here, the decrease is not as sharp as seen earlier for the sample pre-treated in absence of 2-MBI (Figure 3a). This could be due to two factors: the first is an increase in surface roughness, as attested by the other ion profiles in Figure 3b, the second is that the chloride ions interact with the inner layers too thus maintaining a higher intensity for the $^{37}Cl^-$ ion profile even until 400 seconds of sputtering time. This is investigated further by XPS analysis of the surfaces.

The XPS core level spectra recorded for the two cathodically pre-treated copper surfaces, normalized to the background at the lower binding energy side, are shown in Figure 4. The intensities for the S 2p and Cl 2p spectra of curve (a), and the O 1s spectra of curve (b) are multiplied by a factor of 3 for better perceptibility of the decomposition of the peaks and the components observed.

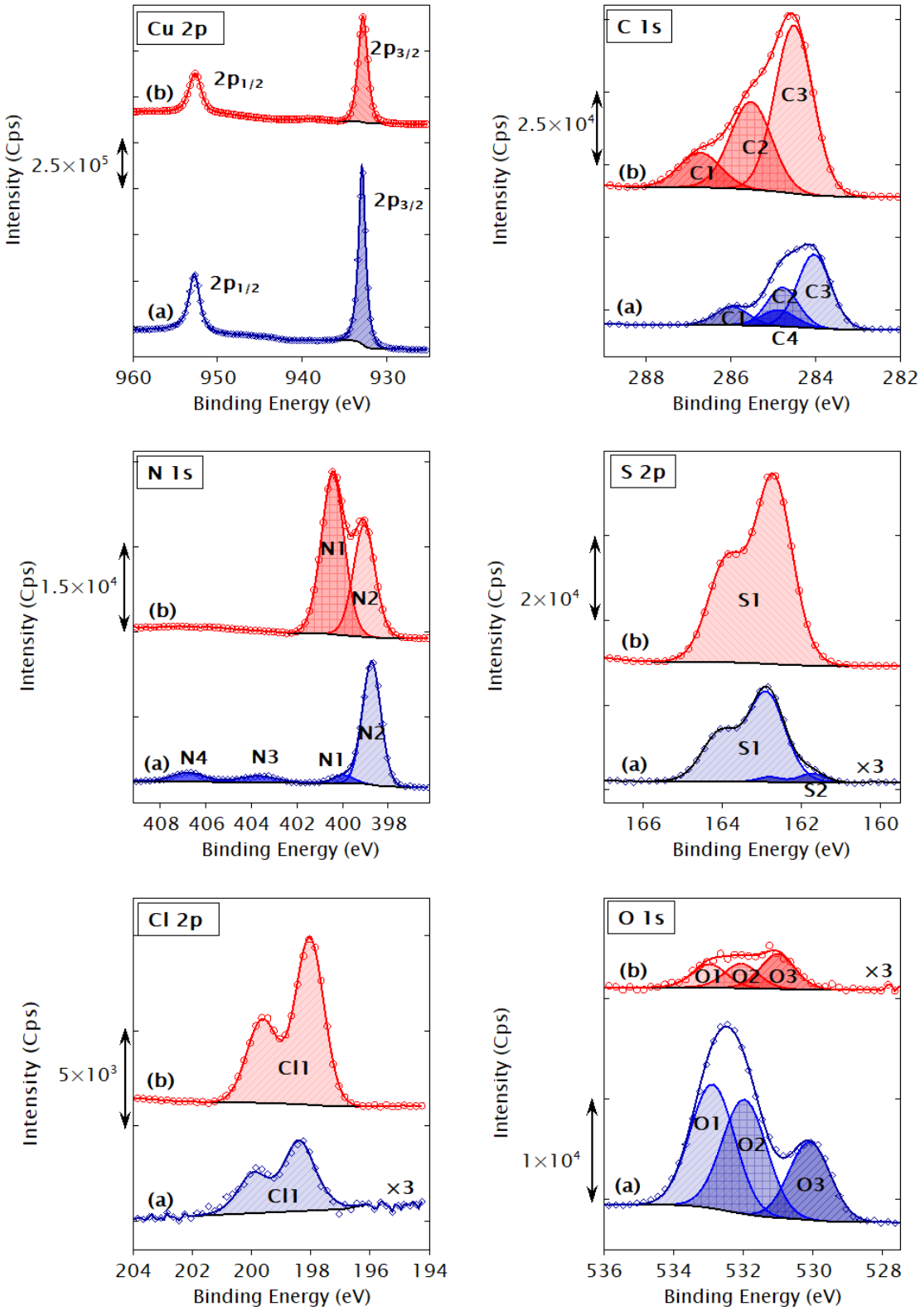


*Figure 4: XPS Cu 2p, C 1s, N 1s, S 2p, Cl 2p, and O 1s core level spectra for 2-MBI films formed on copper surfaces at the reduced state in 10 mM HCl solution after cathodic pre-treatment (a) in the absence of 2-MBI followed by 1 hour exposure to 2-MBI (blue curves), and (b) in the presence of 2-MBI (red curves). The symbols represent the experimental data and the*

*corresponding coloured lines represent the fit. Intensities are normalised to the background at the lower binding energy side.*

The Cu 2p spectra exhibit spin-orbit doublets of $2p_{3/2}$ and $2p_{1/2}$ at the binding energies of 932.9 and 952.6 eV, respectively. Since the binding energies of the Cu metal, $Cu_2O$ oxide, and CuS, are very close to each other, as discussed in previous work [43], their contributions overlap and therefore we cannot decompose this peak. Nevertheless, the Cu $2p_{3/2}$ peak for curve (b), corresponding to the sample pre-treated in presence of 2-MBI, exhibits broadening with full width at half maximum (FWHM) of 1.4 eV, compared to 1.0 eV for the sample pre-treated in absence of 2-MBI (curve (a)). This broadening of the FWHM is most likely due to a change in the chemical state of copper that cannot be distinguished by the Cu 2p spectrum alone. We also observe a reduced intensity for curve (b), confirming that the surface layers are much thicker here thus causing larger attenuation of the Cu signal from the substrate. The presence of thicker surface layers for this substrate has also been indicated by the ToF-SIMS depth profiles in Figure 3.

The C 1s spectrum for the sample pre-treated in presence of 2-MBI (curve (b)), was decomposed into three components – C1 at 286.8 eV corresponding to C=S bonds, C2 at 285.6 eV corresponding to C–N bonds, and C3 at 284.6 eV corresponding to the C–C and C–H bonds, like in previous works on 2-MBI adsorption on metallic copper under UHV conditions [21,22]. A closer look at the intensities of these 3 components revealed that the ratio between the 3 peaks is approximately 1:2:4, indicative of the 7 carbon atoms of the 2-MBI molecule and their respective chemical states [21]. This phenomenon is similar to that observed for 2-MBT deposition on copper surfaces in varying conditions [43–45,50–52].

For the sample pre-treated in absence of 2-MBI (curve (a)), similar fitting parameters were used for decomposition of the C 1s spectrum. This was performed by maintaining the ratio of intensity between the three components and the difference in binding energies between each component. We observe that the binding energies of all the components are lower here by 0.7 ± 0.1 eV, with the C1 at 286 eV, C2 at 284.7 eV, and C3 at 284 eV. The lower binding energies obtained here have also been reported in previous work on adsorption of 2-MBI on pre-oxidized copper surfaces in vapour phase [21,22]. Since the shift is observed for all three components while keeping the relative position of the components between each other within the uncertainty range of ± 0.1 eV, it is understood that this phenomenon is not due to

a change of the chemical states. Rather, this shift is most likely due to a change in the Fermi level of the elements due to bad conductivity between regions of the surface layers and the XPS analyser. This causes an uneven charge compensation for each layer (organic and oxide layers, as discussed below) that is formed on the metallic substrate, thus resulting in shifted binding energies for the components. The binding energy values obtained for the carbon components are reproducible, thus confirming that it is not due to any experimental anomaly.

A fourth component is realised in the C 1s spectrum for the sample pre-treated in absence of 2-MBI (curve (a)) at approximately the same binding energy as that of the C–N bonds, at 284.6 eV. This component arises due to one of the following two reasons. The first possibility is that this component occurs from contaminations on the surface during the *ex-situ* transfer of the sample in air. The second possibility is that there may be an excess of C–N bonds due to partial dissociation/fragmentation of the 2-MBI molecule, thus resulting in an increased intensity at 284.6 ± 0.1 eV.

Lastly, we observe that the intensity of the C 1s spectrum obtained for the sample pre-treated with 2-MBI (curve (b)) is more than twice the intensity for the sample pre-treated in absence of 2-MBI (curve (a)). This agrees with the ToF-SIMS analysis where we observed a thicker overall organic layer on the surface of the sample pre-treated with 2-MBI (Figure 3b).

The N 1s spectrum for curve (a) exhibits 4 chemical states. The N1 component at 400 eV corresponds to nitrogen from 2-MBI not bonded to metallic Cu [21,22]. The N2 component at 398.7 eV is representative of an interaction between nitrogen and metallic copper, as seen in previous work where 2-MBI was adsorbed on a clean metallic surface of copper in vapour phase [21,22]. The intensity of the N2 component is much higher than for the N1 component, suggesting that most of the nitrogen bonds with metallic copper. The formation of thicker multi-layers is restricted here despite exposing the surface to the 2-MBI containing solution for a longer time (1 hour). The atomic ratio of N1/Cu is 0.006 while that of N2/Cu is 0.080, given in Table 2, demonstrating that the intensity of N1 is approximately 13 times less than that of N2. The N3 component at 403.7 eV corresponds to the presence of azides [53], while the N4 component at 406.8 eV corresponds to the formation of nitrates [53]. Although it is unclear why these species are formed here, an explanation would be that due to the partial dissociation of the 2-MBI molecule during adsorption, the free nitrogen interacts with other species available such as oxygen or other free nitrogen-carbon chains to form these species.

*Table 2: Atomic ratios obtained by quantitative analysis of the XPS measurements at the reduced state using the photoelectron intensities, normalised by the photoionization cross-sections, the inelastic mean free paths, and the transmission function of the analyser.*

| **Component** | Pre-treatment without 2-MBI, 1 hour exposure to 2-MBI | Pre-treatment with 2-MBI |
|---|---|---|
| N1/Cu | 0.006 ± 0.001 | 0.44 ± 0.02 |
| N2/Cu | 0.080 ± 0.003 | 0.30 ± 0.01 |
| N/Cu | 0.086 ± 0.003 | 0.74 ± 0.03 |
| S1/Cu | 0.046 ± 0.001 | 0.44 ± 0.01 |
| S2/Cu | 0.003 ± 0.001 | – |
| S/Cu | 0.049 ± 0.001 | 0.44 ± 0.01 |
| O3/Cu | 0.038 ± 0.002 | 0.017 ± 0.001 |
| O/Cu | 0.164 ± 0.007 | 0.039 ± 0.002 |
| Cl/Cu | 0.011 ± 0.001 | 0.24 ± 0.01 |

For the sample pre-treated with 2-MBI, curve (b), we observe only two peaks – N1 and N2. A positive shift of 0.4 ± 0.1 eV for the binding energies is observed, but the relative positions of the 2 components with each other remain the same, as observed for the carbon spectra. These binding energies for nitrogen, N1 at 400.4 eV and N2 at 399.1 eV, are similar to those obtained for 2-MBI adsorption on pre-oxidized copper (3D oxide) under UHV conditions [21]. Since the binding energies differ from the previous case, it is suggested that the chemical state of the nitrogen on this sample may be altered. Therefore, we propose that the N2 component here corresponds to N bonded to Cu(I) ions, which are dissociated by the conversion reaction of the oxide during cathodic pre-treatment, while the N1 component corresponds to N in the physisorbed multi-layers of the organic layer. It is also seen that the N1 component for curve (b) is significantly higher with the N1/Cu ratio of 0.44 versus the N2/Cu ratio of 0.30 (Table 2), supporting the presence of multi-layers of 2-MBI and also confirming the presence of a thicker organic layer than on the previous sample (curve (a)).

The S 2p spectra were decomposed by considering their spin orbit doublets of $2p_{3/2}$ and $2p_{1/2}$ with a branching ratio of 0.5 and splitting of 1.18 eV. For the sample pre-treated in absence of 2-MBI (curve (a)), two components were observed – S1 and S2. The S1 component at 162.9 eV, for the $2p_{3/2}$ spin orbit, corresponds to exocyclic sulphur from the 2-MBI molecule that is not bonded with metallic copper [21]. The S2 component at 161.7 eV is representative of the

interaction between metallic copper and sulphur [43,44], which was observed in previous work on adsorption of both 2-MBI and 2-MBT on metallic copper in UHV conditions [21,22,50,51]. Moreover, this S2 component is at the same binding energy as that observed for copper exposed to $H_2S$ gas, resulting in adsorbed atomic sulphur on the surface [54]. The S2 component can appear from the entire molecule, its fragments, and/or even free sulphur dissociated from the molecule, as discussed in previous works of 2-MBT adsorption on copper [43,44,50,51].

On the other hand, the sample pre-treated with 2-MBI, curve (b), exhibits only one component – S1 corresponding to sulphur not bonded to metallic copper. The intensity of the S1 peak for curve (b) is significantly greater than that of curve (a), even though curve (a) has been increased by a factor of 3 to show the spectrum properly. This is reflected in the S/Cu atomic ratio given in Table 2, where the S/Cu ratio for curve (a) is 0.049 and that for curve (b) is 0.44, which is a 9-fold increase in S intensity. Since the S2 component, S bonded to metallic Cu, generally exhibits low intensity due to the restricted availability of the metallic Cu surface, we cannot completely rule out the possibility of a very small S2 component for the sample pre-treated with 2-MBI (curve (b)). This also considers the fact that we do in fact have a nitrogen component, N2, which bonds directly to metallic Cu in this case. Therefore, sulphur bonding with the metallic substrate cannot be excluded here. Moreover, we did observe copper-sulphur interaction on this sample from the ToF-SIMS depth profile in Figure 3b at a greater sputtering time than copper-nitrogen interaction. Regardless, even if this S2 component is present for curve (b), its intensity is less than 1% of the total intensity of sulphur thus rendering it negligible for quantitative analysis.

From the C 1s spectra it is suggested that we may have some fragmentation of the 2-MBI molecule upon adsorption. In previous works, it was also demonstrated that there is some free atomic sulphur due to dissociation of the inhibitor molecule, for both 2-MBI and 2-MBT [21,22,43,44,50,51]. To determine this, we calculate the atomic ratios between sulphur, nitrogen, and carbon using the intensities obtained from XPS and relate them to the stoichiometric ratio of atoms from the 2-MBI molecule. It is observed that for the sample pre-treated in the absence of 2-MBI, corresponding to spectra (a), we have 1.25 ± 0.06 sulphur atoms and 2.17 ± 0.02 nitrogen atoms, assuming the carbon intensity corresponds to the 7 carbon atoms of the molecule. This confirms that we have an excess of sulphur atoms present

here along with some fragmented nitrogen from the 2-MBI molecule. For the ratios mentioned above, we have only considered the intensities corresponding to the molecule itself, i.e. we have ignored the contributions from the N3, N4, and the C4 components relating to the azides, nitrates, and the excess contamination, as discussed earlier.

Similarly, for the sample pre-treated in the presence of 2-MBI, corresponding to spectra (b) in Figure 4, we estimate that we have 1.21 ± 0.06 sulphur atoms and 2.05 ± 0.02 nitrogen atoms for the 7 carbon atoms. This indicates that again there is an excess of sulphur atoms here. Regarding the nitrogen atoms, the ratio determined is very close to the stoichiometric ratio of the molecule. Therefore, using this pre-treatment method (with 2-MBI) results in fragmentation of the molecule too, but mostly sulphur dissociation and very little nitrogen dissociation, unlike for pre-treatment without 2-MBI followed by 1 hour exposure to 2-MBI. This would also explain why we have a strong intensity for the $CuS^-$ ion profile for a longer sputtering time compared to the $CuN_2^-$ ion profile, from the depth profiles in Figure 3b. The partial decomposition of the 2-MBI molecule was also observed in the work of Whelan et al. [55] on 2-MBI adsorption on a gold (Au(111)) surface. They concluded that when 2-MBI interacts directly with metallic Au, partial decomposition of the molecule occurs resulting in the formation of atomic sulphur. However, they did not note any excess nitrogen from partial decomposition, unlike our case, possibly due to differing experimental conditions.

The Cl 2p spectra, decomposed by their spin-orbit doublets $2p_{3/2} - 2p_{1/2}$ with a branching ratio of 0.5 and splitting of 1.6 eV, exhibit only one component (Cl1) at a binding energy of 198.2 eV. This Cl1 component has been assigned to adsorbed chloride [53], as seen and discussed in previous works [43,45]. Although we cannot rule out the formation of $CuCl/CuCl_2$ due to decomposition limitations arising from the low intensity of the spectra, the absence of a distinct peak is rather interpretative in itself. It suggests that despite the aggressive nature of the electrolyte, strongly acidic with chloride ions, the 2-MBI organic inhibitor is always preferably bonded to the substrate over chloride ions, despite the variations in the bonding mechanisms or the structure of the film. Nevertheless, the atomic ratio of adsorbed chloride is 0.011 for the sample pre-treated in absence of 2-MBI compared to 0.24 for the sample pre-treated in presence of 2-MBI, as seen in Table 2. This suggests that the former pre-treatment is more effective in protecting the surface from chloride ions, despite the lower thickness of the 2-MBI organic layer formed on the substrate as suggested by the N 1s and S 2p scans of

spectra (a). This interpretation was also obtained from the ToF-SIMS depth profiles earlier, Figure 3, where we saw deeper penetration of chloride ions for sample (b) compared to sample (a) in terms of sputtering time.

The O 1s spectra of the two pre-treated surfaces are shown in Figure 4. For the sample pre-treated in absence of 2-MBI, curve (a), the spectrum was decomposed into 3 peak components. The O1 component at 532.9 eV corresponding to adsorbed water, O2 at 532 eV indicative of hydroxides, and O3 at 530.1 eV corresponding to metal oxide ($Cu_2O$) [43,44,54]. The O3/Cu atomic ratio obtained for this sample is 0.038, indicating a low quantity of oxides present here due to the efficiency of the pre-treatment used. This was also observed in previous work of 2-MBT adsorption of Cu in acidic conditions using a similar pre-treatment method [43]. The low quantity of oxides was also corroborated by the low intensity of the $CuO^-$ ion in the ToF-SIMS depth profiles seen in Figure 3a. The overall O/Cu atomic ratio is 0.164, thereby demonstrating that the metal oxide component is only $1/4^{th}$ of the total oxygen present.

For the sample pre-treated in presence of 2-MBI, curve (b), the spectrum was decomposed using similar parameters as that for curve (a) and is increased threefold to make the decomposition and the components visible in the graph. We observe three components for this spectrum too. The O1 relates to water adsorbed while the O2 to hydroxides, as mentioned above. These components are found at the same binding energies as those for the previous case. However, we observe a shift of the O3 component to a higher binding energy by approximately 1 eV. This large shift suggests that there is a change in the chemical state of the O3 component here and it is not the same as the O3 component ($Cu_2O$ metal oxide) found in the previous case. The O3/Cu atomic ratio is 0.017 for this sample (pre-treated with 2-MBI), which is half of that observed for the previous case. We also observe that the overall O/Cu atomic ratio is very low compared to the previous case, with a value of 0.039 compared to 0.164 for the previous sample.

Since we know that the pre-treatment method with 2-MBI is not as effective in reducing the native oxides, as indicated from the CVs in Figure 2, it is proposed that the initial copper oxides present on the surface undergo a conversion reaction during cathodic pre-treatment of the surface, resulting in the consumption/release of oxygen from the copper oxides. This reaction then leaves Cu(I) ions free from the oxides which allows them to interact with 2-MBI molecules

to form metal-organic complexes. Therefore, we obtain a much lower intensity for the O 1s spectrum for the sample pre-treated in presence of 2-MBI. The reduced intensity of oxygen for this sample was also observed in the ToF-SIMS depth profiles in Figure 3.

To understand the effect of oxides more clearly, we decomposed the Cu LMM Auger spectra obtained from the XPS analysis for the two experiments (Figure 5). The sample pre-treated in absence of 2-MBI followed by 1 hour exposure to 2-MBI (Figure 5a) exhibits a relatively low Cu(I) intensity, with a ratio of 0.26 ± 0.01 between Cu(I) and Cu(0) components. This is in line with the observations from the O 1s spectrum of this sample where we observed a low quantity of oxides remaining at the interface due to the efficiency of the pre-treatment used.

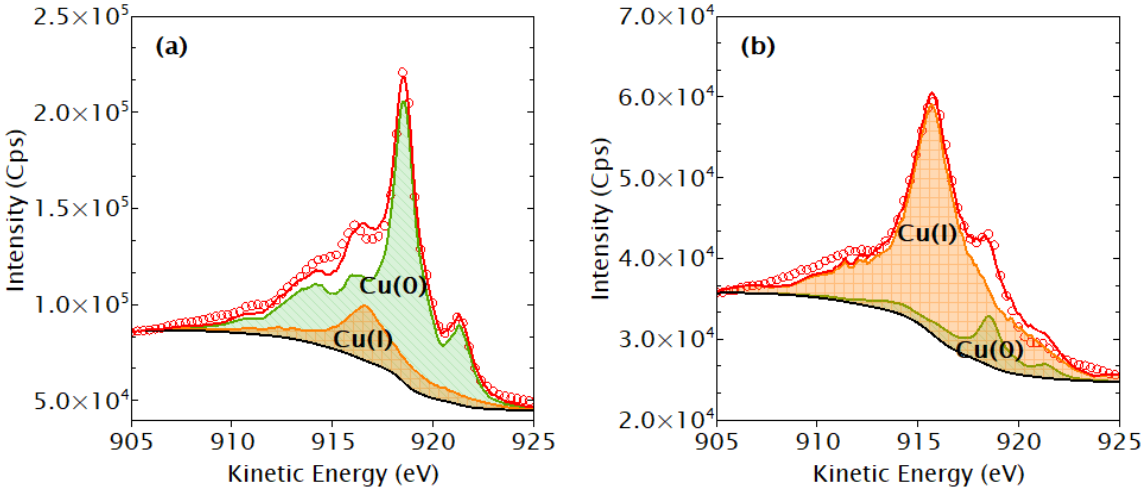


*Figure 5: Cu LMM Auger spectra for 2-MBI films formed on copper surfaces at the reduced state in 10 mM HCl solution after cathodic pre-treatment (a) in the absence of 2-MBI followed by 1 hour exposure to 2-MBI, and (b) in the presence of 2-MBI.*

For the sample pre-treated in presence of 2-MBI (Figure 5b), the Cu LMM Auger scan shows a drastically different profile. The Cu(I) component has a much higher relative intensity here, resulting in a Cu(I)/Cu(0) intensity ratio of 6.11 ± 0.22. Since we did not observe $Cu_2O$ metal oxide in the O 1s spectrum for this sample, Figure 4, it is suggested that the Cu(I) component here is mostly due to the presence of complexes which are formed by the conversion reaction of the copper native oxide during cathodic pre-treatment of the surface in presence of 2-MBI. The Cu(I) ions, released from the initial copper oxides present, interact with the 2-MBI molecules to form the complexes. This inference is in line with the observations from the ToF-SIMS depth profile of this sample seen in Figure 3b, where we observed an initial decrease in

intensity of the $Cu^-$, $O^-$, and $C_7H_4N_2S^-$ ion profiles which was attributed to the presence of complexes on the surface.

The metal organic complexes formed by 2-MBI and copper are quite different than those formed by 2-MBT and copper. As seen in previous works [44,45], the Cu-2-MBT complexes are only formed in neutral and alkaline media, not in acidic media, despite both inhibitors utilizing Cu(I) ions for the formation of the complexes. This was attributed to the dominant conformer of the 2-MBT molecule in each environment. Only the thiolate form of the molecule enabled the formation of the complexes, most likely due to the absence of a hydrogen atom in the molecule thus leaving an extra reactive site for the interaction with the Cu(I) ions. However, in the present case, even though the dominant form of 2-MBI in acidic media is the thione conformer, significant quantities of the metal organic complexes are formed, as evidenced by the Cu LMM Auger spectrum. There can be two possibilities for this occurrence. The first is that the Cu(I) ions replace the hydrogen atoms attached to the nitrogen atoms of the molecule due to stronger affinity between them, thus forming the complexes. The second possibility is that due to some fragmentation of the molecule, there is a new reactive site in the molecule for the Cu(I) ions to interact with, thus forming the complexes. However, we cannot confirm or rule out either hypothesis at this point.

## Corrosion tests and inhibition by 2-MBI organic inhibitor

To investigate the corrosion behaviour of copper in the acidic chloride environment and the inhibition offered by the 2-MBI molecule on various pre-treated surfaces, cyclic voltammetry tests were performed. The CVs are shown in Figure 6 and the corresponding anodic and cathodic charge densities along with equivalent thickness of copper reacting are given in Table 3.

For the sample polarised in the reference 10 mM HCl solution, we observe a sharp increase in current density initiating at approximately 0.15 V vs SHE, corresponding to anodic dissolution of copper metal. The measured charge density for the anodic branch of the polarisation is 7032 ± 13 μC/cm² and the estimated equivalent thickness of reacting copper is 5.17 ± 0.02 nm, also given in Table 3. Subsequently, a cathodic peak corresponding to copper redeposition is observed during reverse sweeping at a potential of 0.08 V vs SHE. The measured cathodic charge density was 4503 ± 55 μC/cm². The large difference between the anodic and cathodic

charge densities indicates a considerable quantity of copper metal irreversibly dissolved during the cyclic voltammetry test, which is estimated to be approximately 1.86 ± 0.03 nm of equivalent thickness.

The copper surfaces with the 2-MBI inhibitor exhibited significantly lower rises in the current density during the anodic branch compared to the reference substrate. To examine the CVs clearly, they are enlarged in Figure 6b. The sample pre-treated in the absence of 2-MBI followed by 2 minutes of exposure to 2-MBI shows an increase in current density initiating at 0.23 V vs SHE, a positive shift of 0.07 V compared to the reference substrate. This indicates a delayed corrosion initiation on the 2-MBI covered surface along with a slower corrosion rate as expressed by the slower rise of current density. When the exposure time was increased to 1 hour for a similarly pre-treated sample, we observed a further positive shift of 0.05 V for corrosion initiation to 0.28 V vs SHE, indicating that the extended exposure time to the inhibitor results in a better protection of the substrate. The positive shifts observed for the two samples also result in progressively lower amounts of copper reacting, as seen in Table 3, due to the inhibitive effect of the 2-MBI molecule.

Lastly, the sample pre-treated in presence of 2-MBI also exhibits a rise in current density starting at 0.28 V vs SHE. However, the increase is much less here than for the previous two samples (pre-treatment without 2-MBI followed by exposure to 2-MBI), with an equivalent thickness of 0.40 ± 0.02 nm of reacting copper estimated from the anodic branch of the CV. This suggests that the sample pre-treated with 2-MBI results in the most protective barrier layer/interface of the three inhibited samples. This is most likely due to the copper oxide–2–MBI interaction resulting in the formation of a conversion layer of protective complexes which further restricts the electrolyte from accessing the metal substrate.

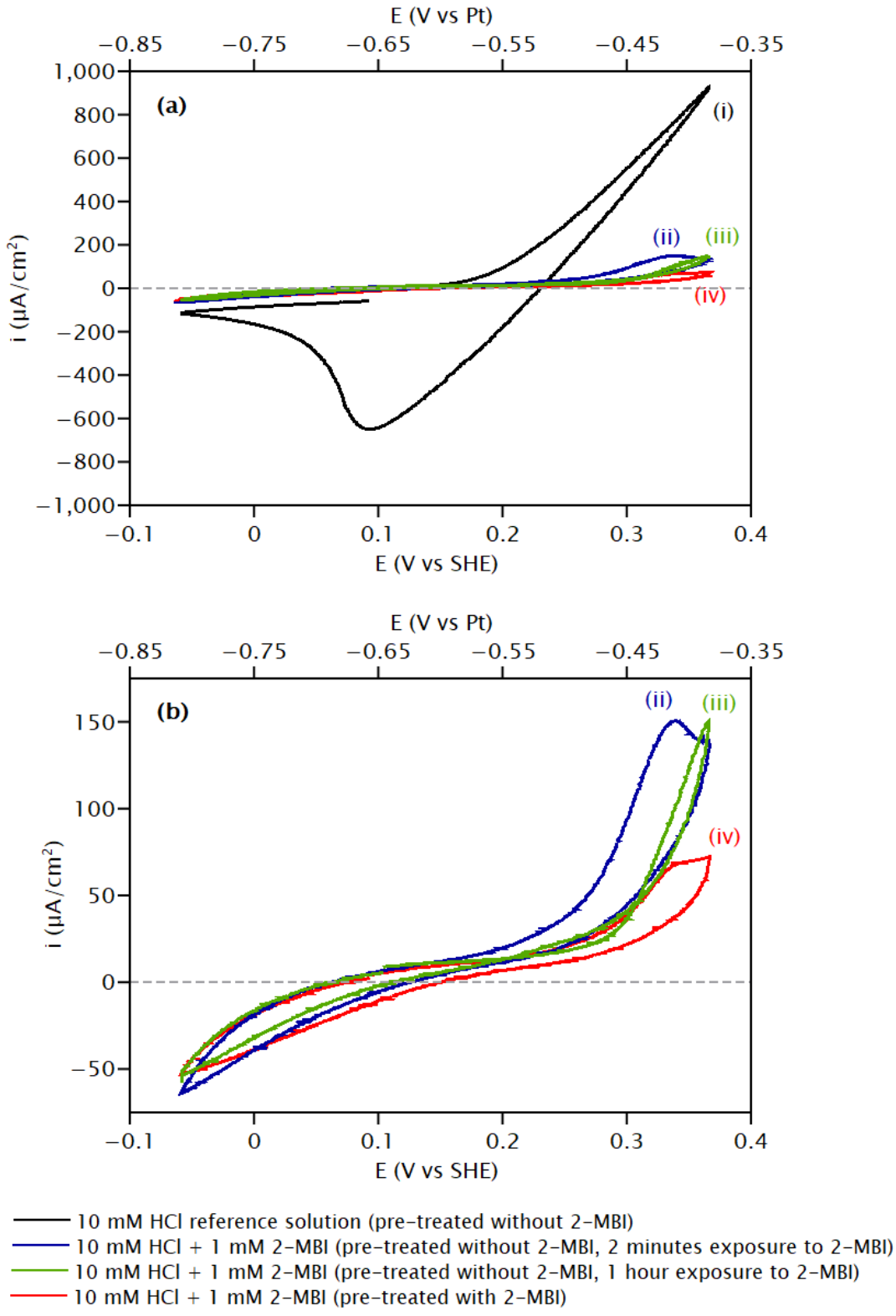


*Figure 6: (a) CV tests of copper anodic dissolution in 10 mM HCl solution in (i) the absence of 2-MBI, and (ii-iv) the presence of 2-MBI, after the various cathodic pre-treatment methods of the interface. (b) Enlarged CVs of the copper surfaces polarised in the presence of 2-MBI.*

*Table 3: Anodic and cathodic charge densities (µC/cm²) determined from the cyclic voltammetry anodic dissolution tests by integrating the current densities measured with time, and equivalent thickness (nm) of copper metal reacting estimated using Faraday's law.*

| | Electrolyte, Pre-treatment method | Anodic charge density (µC/cm²) | Cathodic charge density (µC/cm²) | Equivalent thickness of copper reacting (nm) |
|---|---|---|---|---|
| i | 10 mM HCl reference solution, Pre-treatment without 2-MBI | 7032 ± 13 | 4503 ± 55 | 5.17 ± 0.02 |
| ii | 1 mM 2-MBI + 10 mM HCl, Pre-treatment without 2-MBI, 2 minutes exposure to 2-MBI | 1101 ± 4 | 282 ± 21 | 0.81 ± 0.01 |
| iii | 1 mM 2-MBI + 10 mM HCl, Pre-treatment without 2-MBI, 1 hour exposure to 2-MBI | 839 ± 5 | 216 ± 6 | 0.62 ± 0.01 |
| iv | 1 mM 2-MBI + 10 mM HCl, Pre-treatment with 2-MBI | 541 ± 7 | 296 ± 22 | 0.40 ± 0.02 |

To understand this effect further, cyclic voltammetry was carried out on the sample pre-treated without 2-MBI followed by 1 hour exposure to 2-MBI and on the sample pre-treated with 2-MBI, with an anodic branch extended up to 0.75 V vs SHE (Figure 7). We observe that for the sample pre-treated without 2-MBI followed by 1 hour exposure to 2-MBI, the anodic current density increase, seen earlier in Figure 6, corresponds to a peak at 0.38 V vs SHE with a subsequent decrease until 0.45 V vs SHE. This suggests that the rise in current density relates to a reaction preceding corrosion initiation. Since this peak is absent for the CV obtained for the sample pre-treated with 2-MBI, it is likely that the reaction responsible for this effect has already occurred on this latter sample during cathodic pre-treatment of the surface, i.e. by consuming the oxygen atoms from the native oxide thus leaving the Cu(I) ions to interact with 2-MBI to form Cu(I)-2-MBI complexes.

Therefore, we propose that the peak observed for the sample pre-treated without 2-MBI followed by 1 hour exposure to 2-MBI at 0.38 V vs SHE is associated with the interaction between Cu(I) ions, formed during anodic polarisation in this case, and 2-MBI molecules, resulting in the formation of a metal-organic complex that prolongs the corrosion inhibition

up until a slightly higher potential. The main distinction in the formation of the complexes for the two samples is that on the sample pre-treated with 2-MBI, the Cu(I) ions originate from the native oxide film and are released during the cathodic pre-treatment cycles while for the sample pre-treated without 2-MBI, the Cu(I) ions are formed by anodic oxidation of copper metal and thus the complexes are formed at a later stage.

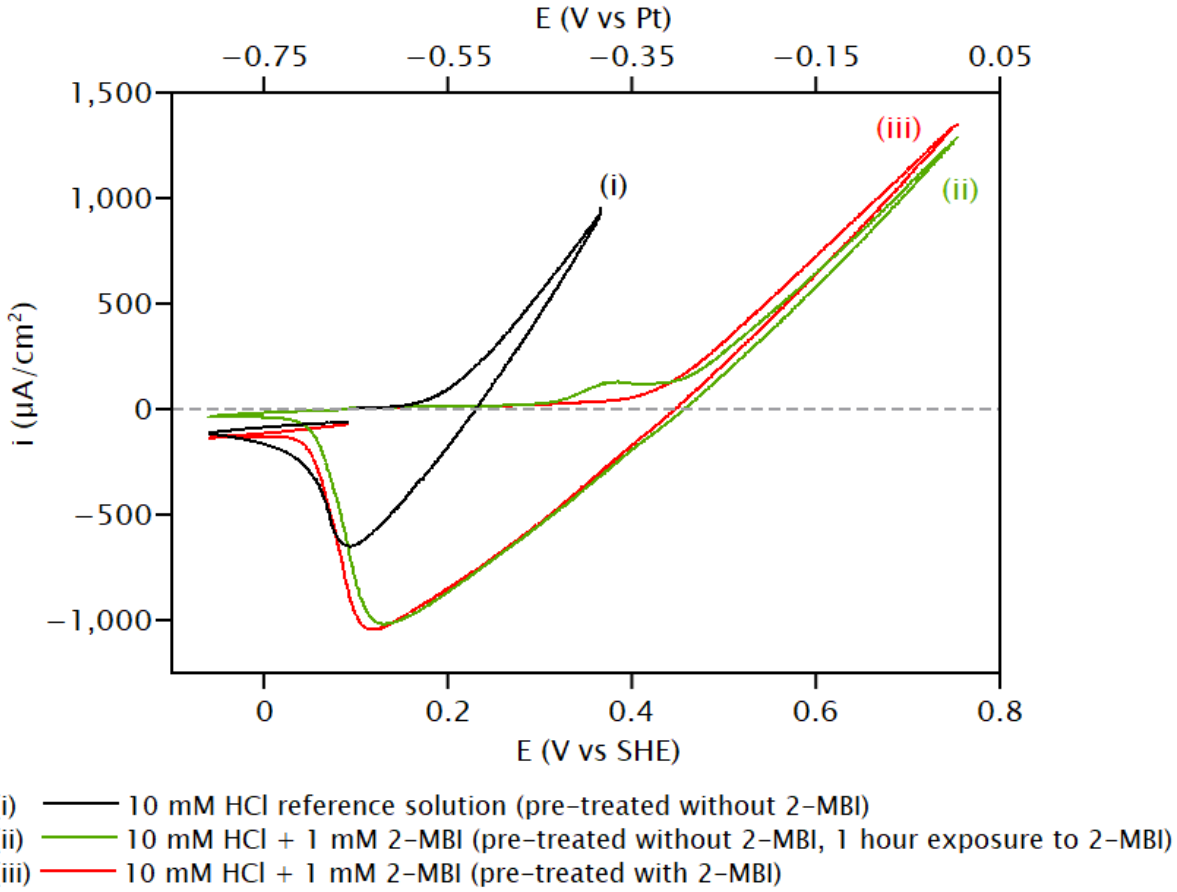


*Figure 7: CV tests of copper anodic dissolution with extended anodic range in 10 mM HCl + 1 mM 2-MBI in (i) the absence of 2-MBI, and (ii-iii) the presence of 2-MBI, after the various cathodic pre-treatment methods of the interface.*

The corrosion initiation, on the other hand, occurs later at a potential of 0.45 V vs SHE, indicated by a sharp rise in current density, while that of the sample pre-treated in 2-MBI was observed at 0.28 V vs SHE. Therefore, the sample pre-treated without 2-MBI followed by 1 hour exposure to 2-MBI does in fact protect the substrate for a greater potential range, indicating that the inner chemisorbed layer formed is more restrictive against the electrolyte for this sample. This is in agreement with the work on 2-MBT adsorption on copper [43,45], where the samples pre-treated in absence of the inhibitor followed by exposure to the

inhibitor also yielded superior barrier layers in terms of protection against corrosion compared to the samples pre-treated in presence of the inhibitor.

In previous work where 2-MBT was used as an inhibitor for copper in acidic chloride media [43], it was established that the 2-MBT organic molecule is exceptionally effective for corrosion inhibition of copper. Since the present work was carried out in similar conditions, we can make comparisons between the corrosion inhibition effectiveness of the two different organic molecules on copper. In the present work, we observe that the sample pre-treated in presence of 2-MBI exhibits a reduction in anodic current density of approximately 92.25% at 0.37 V vs SHE (anodic peak), whereas the sample pre-treated in absence of 2-MBI followed by 1 hour exposure to 2-MBI exhibits a reduction of approximately 83.87%. Although we have seen and discussed the effects of the conversion peak in the latter sample, we are considering the anodic current density values at 0.37 V vs SHE for ease of comparison. On the other hand, for the 2-MBT molecule on copper in acidic chloride media, the sample pre-treated with 2-MBT obtains a 74.20% reduction while the sample pre-treated without 2-MBT followed by 1 hour exposure to 2-MBT obtains an astonishing 99.75% reduction in anodic current density at the same potential (0.37 V vs SHE)[43].

The above figures demonstrate that with a better control of the surface and/or interface of the copper sample, 2-MBT achieves a better result on the protection of copper metal from corrosive attack in an acidic chloride media. Additionally, the concentration of 2-MBT used was 0.1 mM due to its very low solubility in acidic media, whereas the concentration of 2-MBI used in the present work was 1 mM, an increase by a factor of 10. This in turn shows that even in lower concentrations, 2-MBT is more effective on copper than 2-MBI as an inhibitor.

### Effects of anodic polarisation on the 2-MBI barrier layer by surface analysis

The ToF-SIMS depth profiles obtained at the anodic state of the sample, i.e. anodically polarised to 0.37 V vs SHE, are shown in Figure 8. The plotted ion profiles and the defining position of each interface/layer is consistent with the depth profiles at the reduced state, presented above in Figure 3.

Using the same criteria based of maximum peak intensity of the $Cu^-$ ion profile, it is observed that the sputtering time taken to reach the Cu substrate for either sample has immensely increased compared to the reduced state. For the sample pre-treated in absence of 2-MBI

(Figure 8a), the increase is approximately 6 times, reaching the metallic copper substrate at 716 seconds of sputtering time. For the sample pre-treated in presence of 2-MBI (Figure 8b), the increase is approximately 3.6 times, reaching the substrate at 2403 seconds of sputtering. The sequence of intensity maxima from the surface to the copper substrate remains the same for either sample with copper–sulphur interaction found at a greater sputtering time than copper–nitrogen interaction. Additionally, the coincidence of the maxima of the copper oxides and copper–sulphur interaction peaks are also seen here.

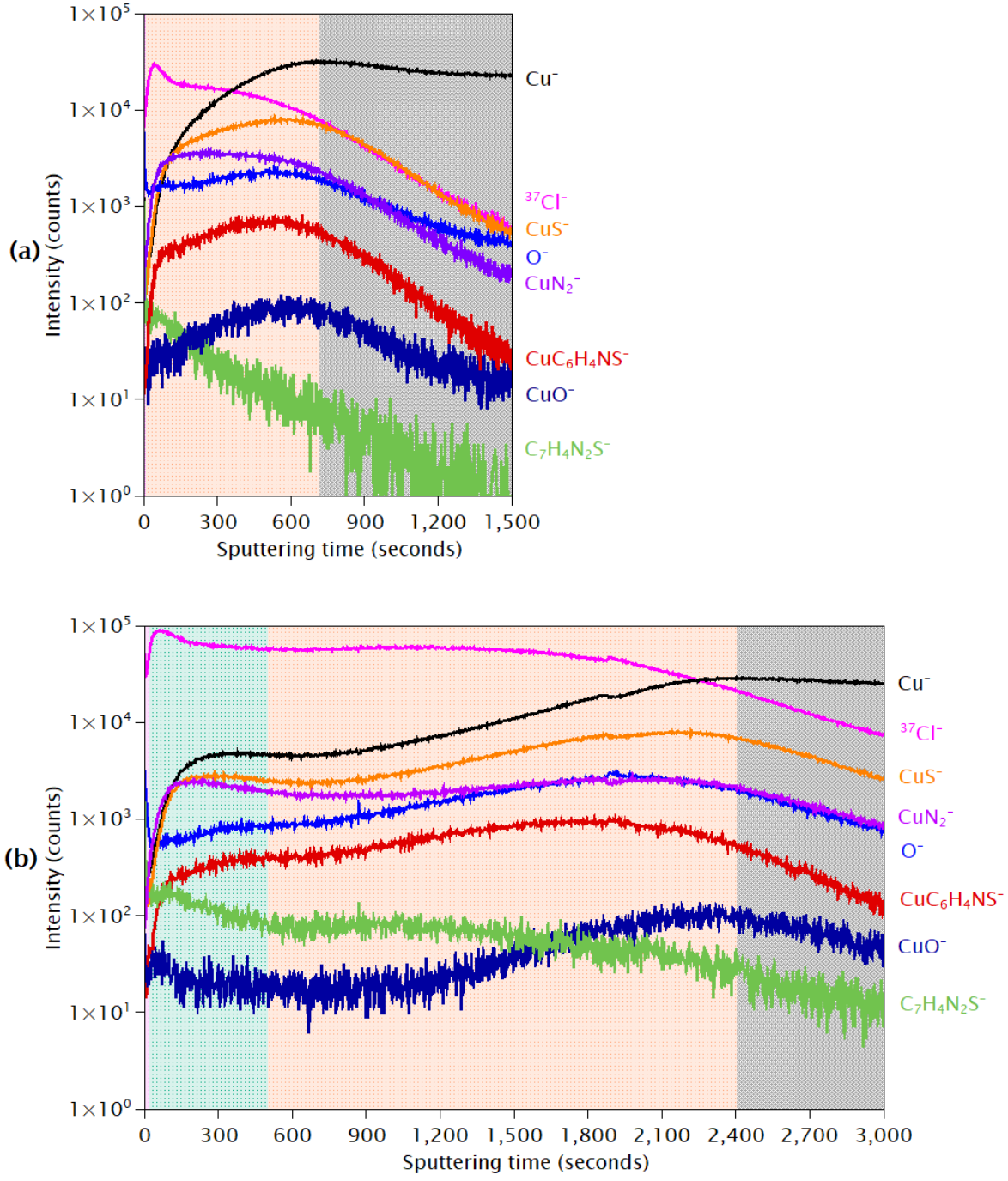

*Figure 8: ToF-SIMS depth profiles obtained after anodic polarisation to 0.37 V vs SHE (anodic state) in 10 mM HCl + 1 mM 2-MBI solution for copper surfaces pre-treated (a) in the absence of 2-MBI followed by 1 hour exposure to 2-MBI, and (b) in the presence of 2-MBI. Intensity in counts (logarithmic scale) vs sputtering time in seconds.*

An interesting feature observed for the sample pre-treated with 2-MBI is that for most ion profiles we observe an initial peak within the range of the first 500 seconds of sputtering (at 330 seconds for the $Cu^-$ ion profile), followed by an inner wave of higher intensity in the range of 1800 – 2500 seconds of sputtering time. Although surface roughness could play a role here, the effect it has is generally on the shape of the ion profile, i.e. slow and creeping instead of sharp profiles. Here, we observe on both samples that the depth profiles exhibit a rather slow decrease in their ion intensities, indicating surface roughness is prevalent. From the extended anodic CVs in Figure 7, we have deduced that corrosion has initiated on the sample pre-treated with 2-MBI but not on the sample pre-treated in the absence of 2-MBI. Therefore, we propose that the outer peaks correspond to the non-homogeneously attacked depth of the sample, where the locally attacked and not yet attacked regions coexist, while the inner waves relate to a greater depth from the surface, beyond the depth of the non-homogeneous corrosive attack. Such an effect of an outer peak and an inner wave in the depth profiles has also been observed by Seyeux et al. [56] where they used ToF-SIMS to characterize the interface between the oxide film of stainless steel and non-homogeneously covering bacteria on the surface.

Another notable feature, this time for the sample pre-treated in absence of 2-MBI (Figure 8a), is the decrease in intensity for the $CuO^-$ ion profile from the reduced state to the anodic state. This is consistent with the fact that the residual copper oxides trapped between the organic layer and the copper substrate are converted by reaction with the 2-MBI molecules and its fragments to form metal-organic complexes leaving only traces of copper oxides. However, we know that this is not the primary mechanism of complex formation for this pre-treatment method. Most of the complexes formed for the sample pre-treated in absence of 2-MBI result from anodic polarisation when the copper metal is oxidized to form Cu(I) ions which then interact with the 2-MBI molecules. Lastly, we observe that the chloride ions, represented by the $^{37}Cl^-$ ion profile, has penetrated considerably into the substrate for both experiments, although this effect is much larger for the sample pre-treated with 2-MBI (Figure 8b).

The XPS spectra obtained for the two surfaces at the anodic state are shown in Figure 9. Like for Figure 4, curve (a) of the spectra relates to the sample pre-treated in absence of 2-MBI followed by 1-hour exposure to 2-MBI, whereas curve (b) corresponds to the sample pre-treated in presence of 2-MBI. The intensities of the Cl 2p spectrum of curve (a) and O 1s spectrum of curve (b) have been increased threefold for better visibility of the decomposition and the components. The decompositions of the spectra have also been detailed earlier.

The Cu 2p spectra exhibits their $2p_{3/2}$ peaks at 932.9 eV for both samples, like for the reduced state. However, the FWHM of the $2p_{3/2}$ peak for the sample pre-treated in absence of 2-MBI followed by 1 hour exposure to 2-MBI (curve (a)) has increased from 1 eV to 1.4 eV, which is similar to that of the sample pre-treated with 2-MBI at the reduced and anodic state, indicating that there is a change in the components upon polarisation. This was also attested by the change in ToF-SIMS depth profiles before and after polarisation, as seen in Figure 3a and Figure 8a. Additionally, a reduction in intensity of the Cu $2p_{3/2}$ peak is observed here, assigned to the increased thickness of organic surface layers, as confirmed by the depth profiles, resulting in a larger attenuation of the substrate signal. For the sample pre-treated in presence of 2-MBI (curve (b)), there is almost no difference observed in terms of BE or FWHM for the Cu 2p spectra before and after anodic polarisation, signifying that the induced changes are either insignificant or that they transpire at a depth greater than the probing depth of the XPS.

Regarding the C 1s spectra, we observe that there is a positive shift in the binding energies of all the components of 0.5 ± 0.2 eV compared to that at the reduced state for both the samples. Additionally, the ratio between the components has been slightly altered. The relative intensity of the C1 component corresponding to the C=S bond has decreased for both samples at the anodic state possibly due to cleavage of the C=S bond induced by anodic polarisation. Therefore, we see a slight relative gain in the intensities of the C2 and C3 components of the C 1s spectra. Although we do not know the exact reason for the shift in binding energies of the carbon components, it is likely that it occurs due to the increased thickness of the 2-MBI organic layer from the formation of complexes upon polarisation, thus causing a positive shift in the binding energies due to bad conductivity between the surface layers corresponding to carbon and the XPS analyser.

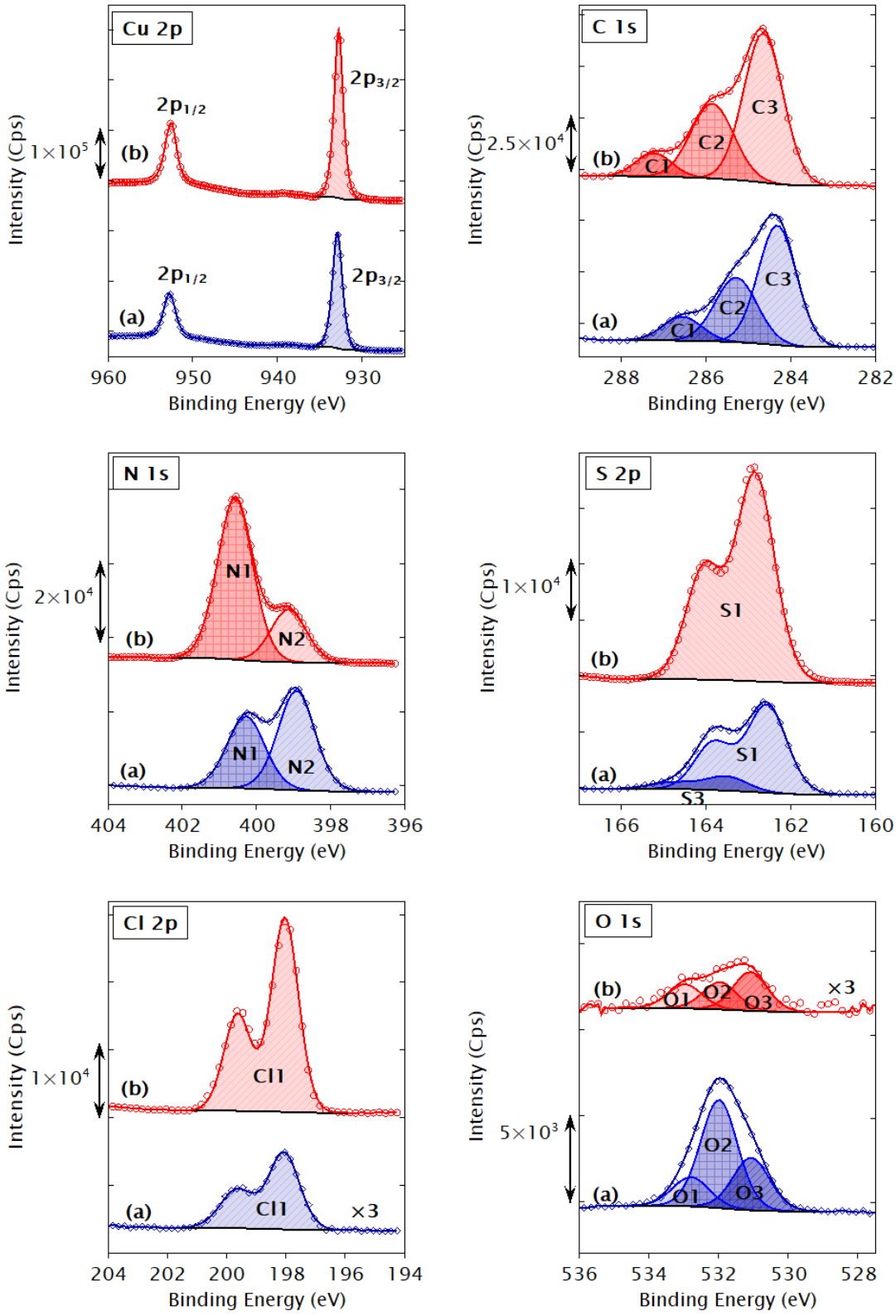


*Figure 9: XPS Cu 2p, C 1s, N 1s, S 2p, Cl 2p, and O 1s core level spectra obtained after anodic polarisation to 0.37 V vs SHE (anodic state) in 10 mM HCl +1 mM 2-MBI solution with for copper surfaces pre-treated (a) in the absence of 2-MBI followed by 1 hour exposure to 2-MBI (blue curves), and (b) in the presence of 2-MBI (red curves). The symbols represent the*

*experimental data and the corresponding coloured lines represent the fit. Intensities are normalised to the background at the lower binding energy side.*

The N 1s spectra of the two samples exhibit 2 peak components here, N1 corresponding to nitrogen not bonded to metallic copper and N2 corresponding to nitrogen bonded to metallic copper. We do not observe the N3 and N4 components here for the sample pre-treated in absence of 2-MBI (curve (a)), unlike at the reduced state. This is in line with the absence of the C4 peak in the C 1s spectrum for the corresponding sample. An increase in the binding energies is noted for the two nitrogen components for both samples. For the sample pre-treated with 2-MBI, the increase in BE is a mere 0.1 eV, which is within the uncertainty range. However, for the sample pre-treated without 2-MBI, the increase in BE is 0.2 eV, suggesting a possible change in the chemical state. We also observe an increase in FWHM of 0.2 eV for the N1 and N2 components for this sample. This increase in BE and FWHM is most likely due to the formation of the metal-organic complexes which alters the chemical state of the nitrogen, from the initial interaction with metallic Cu at the reduced state to the subsequent interaction with Cu(I) ions at the anodic state. For the sample pre-treated with 2-MBI, the interaction between copper and nitrogen at the reduced state was already due to the Cu(I) ions released from the oxides, thus the change is negligible. Lastly, an increase in the intensities of the N1 and N2 components relative to the Cu intensity is observed for both samples, as seen in Table 4. This indicates that we have increased bonding between nitrogen and metallic Cu and/or Cu(I) ions (N2 component), and thicker multilayers of physisorbed 2-MBI not bonded to Cu (N1 component).

In the S 2p spectrum of the sample pre-treated in presence of 2-MBI (curve (b)), we observe only one component, S1 corresponding to sulphur not bonded to metallic copper. The ratio of this component relative to Cu has increased from 0.44 at the reduced state to 0.51 at the anodic state, confirming the presence of a thicker physisorbed layer. Meanwhile, for the sample pre-treated in absence of 2-MBI (curve (a)), we observe that the S2 component at 161.7 eV related to sulphur bonded to metallic copper is absent. Instead, another component, S3, is found at a binding energy of 163.5 eV ($2p_{3/2}$ peak). It is proposed that this S3 component is possibly due to a change in the oxidation state of sulphur from the S2 component seen at the reduced state, and thus results in a change of the binding energy of the species. However, the true nature of this species is not known to us. The S1 peak for curve (a) exhibits an

increased intensity with respect to the Cu intensity, from 0.046 at the reduced state (Table 2) to 0.34 at the anodic state (Table 4). A decrease of 0.3 eV in the BE is also seen for this sample. These observations are in line with that of the nitrogen spectra for the same sample suggesting a change in the chemical state of the molecule and the thicker chemisorbed inner layer after anodic polarisation.

*Table 4: Atomic ratios obtained by quantitative analysis of the XPS measurements at the anodic state using the photoelectron intensities, normalised by the photoionization cross-sections, the inelastic mean free paths, and the transmission function of the analyser.*

| **Component** | Pre-treatment without 2-MBI, 1 hour exposure to 2-MBI | Pre-treatment with 2-MBI |
|---|---|---|
| N1/Cu | 0.30 ± 0.01 | 0.65 ±0.03 |
| N2/Cu | 0.41 ± 0.02 | 0.21 ± 0.01 |
| N/Cu | 0.71 ± 0.03 | 0.86 ± 0.03 |
| S1/Cu | 0.34 ± 0.01 | 0.51 ± 0.02 |
| S3/Cu | 0.057 ± 0.002 | - |
| S/Cu | 0.40 ± 0.01 | 0.51 ± 0.02 |
| O3/Cu | 0.045 ± 0.002 | 0.011 ± 0.001 |
| O/Cu | 0.164 ± 0.007 | 0.025 ± 0.001 |
| Cl/Cu | 0.11 ± 0.01 | 0.53 ± 0.02 |

Similar to the reduced state Cl 2p spectra (Figure 4), the anodic state Cl 2p spectra for the two samples (Figure 9) exhibit one component, Cl1 at 198.2 ± 0.2 eV, corresponding to adsorbed chlorine. However, there is a substantial increase in the Cl intensity from the reduced state to the anodic state for both the samples with respect to the Cu intensity, from 0.011 to 0.11 for the sample pre-treated in absence of 2-MBI (curve (a)), and from 0.24 to 0.53 for the sample pre-treated in presence of 2-MBI (curve (b)). This is in agreement with the ToF-SIMS depth profiles (Figure 8) that show increased intensity of the $^{37}Cl^-$ ion profile for a larger sputtering time compared to that at the reduced state (Figure 3) for both samples. The increased intensity of chlorine insinuates that the 2-MBI organic layer, which consists of the chemisorbed layer including the metal-organic complexes and the physisorbed layer, is not entirely protective. Chloride ions do penetrate the organic layer to interact with the residual oxides and the metallic copper substrate, which can lead to attack. Although the acidic pH of the solution also plays a role in this attack, we have found that under the same conditions of

organic layer formation in a similar media [43], 2-MBT is a more effective inhibitor against copper corrosive attack than 2-MBI.

Lastly, the O 1s spectrum for the sample pre-treated in absence of 2-MBI (curve (a)) exhibits a similar intensity for the overall oxygen content (Table 4) as that at the reduced state (Table 2) with respect to the copper intensity. However, there is a change in intensities among the three components of the O 1s spectrum, with a large increase in the O2 component (hydroxides) and a decrease in the O1 component (water adsorbed). The O3 peak has increased only slightly from 0.038 to 0.045, however, there is a large positive shift of 1 eV in the binding energy of this component from 530.1 eV to 531.1 eV. This component is at the same binding energy as the O3 component for the sample pre-treated in presence of 2-MBI at the reduced state, seen earlier in Figure 4, suggesting that the metal oxide initially present has undergone a change in its chemical state.

Meanwhile, for the sample pre-treated in presence of 2-MBI (curve (b)), we observe that there is a slight reduction in the intensity of the oxygen peaks with respect to copper intensity at the anodic state, both individually and overall, compared to the reduced state. However, we did not observe any change in the binding energies of the three components from the reduced state. To deliberate on these observations further, we examine the Cu LMM Auger spectra for both samples (Figure 10).

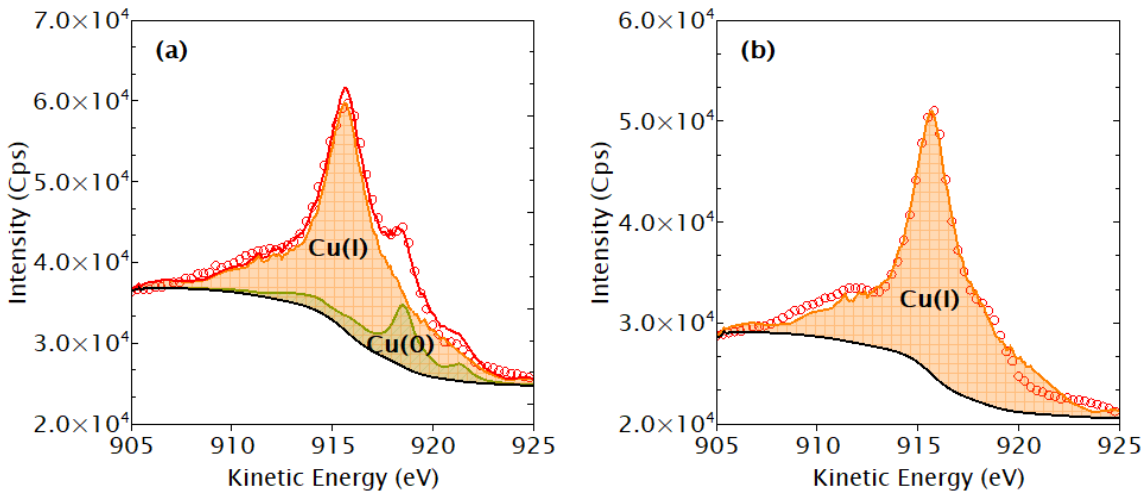


*Figure 10: Cu LMM Auger spectra obtained for 2-MBI films formed on copper surfaces at the anodic state in 10 mM HCl solution after cathodic pre-treatment (a) in the absence of 2-MBI followed by 1 hour exposure to 2-MBI, and (b) in the presence of 2-MBI.*

For the sample pre-treated in absence of 2-MBI followed by 1 hour exposure to 2-MBI (Figure 10a), the Cu(0) component intensity has profoundly decreased while the Cu(I) component is now the major component with a Cu(I)/Cu(0) ratio of 4.86 ± 0.18. However, we did not observe an increase in the oxygen intensity (O 1s) upon polarisation, as discussed above. This suggests that there is an increased formation of metal-organic complexes upon anodic polarisation of the sample, which is also most likely the reason for the shift in BE of the O3 component from the O 1s spectra for this sample. This Cu LMM Auger profile is quite similar to that of the sample pre-treated with 2-MBI at the reduced state (Figure 5b). Additionally, the shifts in BE, increased FWHMs, and the change in atomic ratios observed from the XPS core level spectra for this sample (pre-treated in absence of 2-MBI followed by 1 hour exposure to 2-MBI) suggest that the structure of the organic layer on the sample has changed drastically on anodic polarisation and is likely similar to that of the converted organic layer formed on the sample pre-treated in presence of 2-MBI at the reduced state. This is also consistent with the change of the ToF-SIMS depth profile from the reduced state to the anodic state.

The change in structure of the organic layer of the sample pre-treated in absence of 2-MBI followed by 1 hour exposure to 2-MBI is most likely due to the formation of the complexes on anodic polarisation. Since the sample was pre-treated in absence of 2-MBI, there was no interaction between the molecule and the released Cu(I) ions. Upon anodic polarisation, copper metal is oxidized to Cu(I), which then allows for interactions between the newly produced Cu(I) ions and the 2-MBI molecules. Thus, we obtain a structure similar to that of the sample which was already pre-treated in presence of 2-MBI and formed the metal-organic complex-containing organic layer right at the first cycle of cathodic pre-treatment.

For the sample pre-treated with 2-MBI (Figure 10b), we observe only the Cu(I) component. The absence of Cu(0) from the profile shows that the metallic copper substrate on this sample is below the probing depth of the XPS, although the presence of Cu(0) cannot be completely excluded. This means that the organic layer on this sample, which mostly consists of the complexes, is of a thickness greater than 10 nm as estimated from the TPP-2M formula [48], far greater than the organic layer thickness of 2-MBT adsorbed on copper [43]. This inference also gives validation to our ToF-SIMS results in Figure 8b, where we proposed that the copper substrate is found at a larger sputtering time and the initial peak of the $Cu^-$ ion profile corresponds to the initial top surface of the sample which was non-homogeneously attacked.

The proposed models of the layered structure of the 2-MBI inhibiting interfaces formed at the reduced state and their alteration at the anodic state on both pre-treated Cu substrates are shown in Figure 11. Additionally, the depth of the penetration of the chloride ions on each sample, based on the analysis of the depth profiles obtained by ToF-SIMS, is also shown in the figure. For the sample pre-treated without 2-MBI and subsequently exposed to the inhibitor at the reduced state, the 2-MBI film is bi-layered with inner chemisorbed and outer physisorbed layers and $Cu_2O$ oxide islands trapped at the interface (Figure 11a). The chloride ions have penetrated the outer physisorbed layer, but not the inner chemisorbed layer in this case.

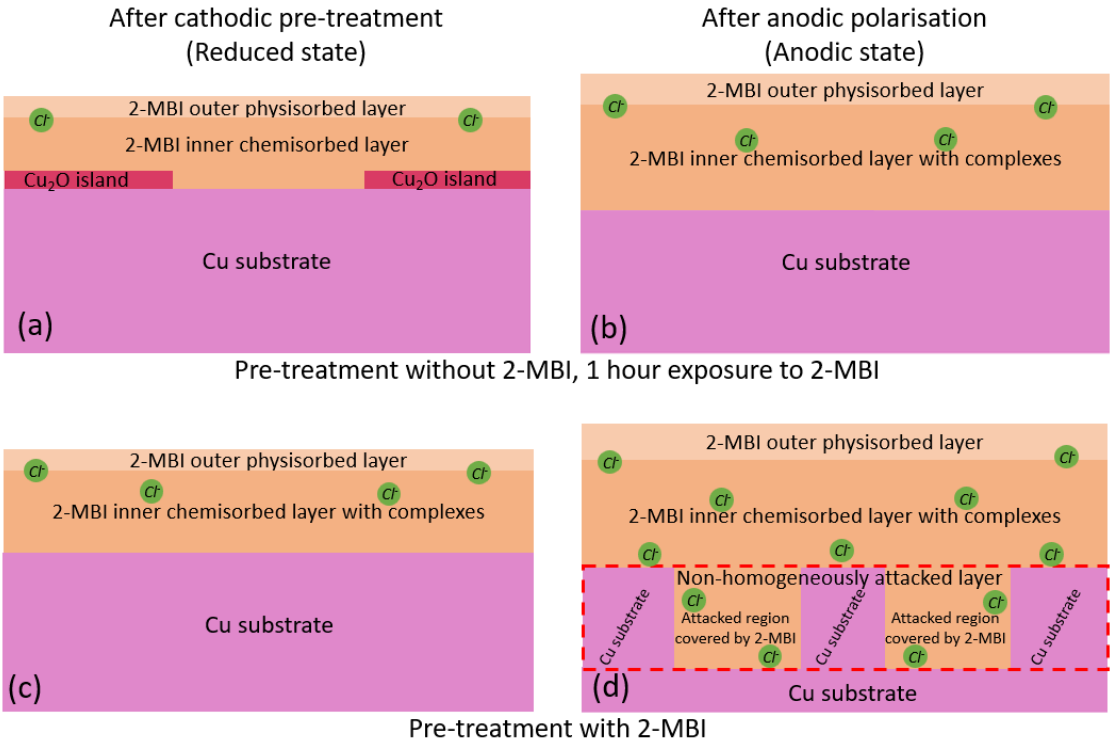


*Figure 11: Bi-layered interfacial structure of the 2-MBI organic films formed on copper in (a,c) reduced and (b,d) anodic states in 10 mM HCl solution for pre-treatment (a,b) in the absence of 2-MBI followed by 1 hour exposure to 2-MBI, and (c,d) in the presence of 2-MBI. The green disks represent the chloride ions that have penetrated the organic film layers, as shown by ToF-SIMS.*

Upon anodic polarisation (Figure 11b), the Cu(I) oxide islands are converted into complexes, as evidenced by the shift in the O3 component binding energy in Figure 9 (curve (a) of O 1s spectrum). Further complexes are formed when Cu(I) ions are produced by anodic oxidation of the metallic Cu substrate, as indicated by the extended CVs in Figure 7 and confirmed by the large intensity of Cu(I) ions from the Cu LMM Auger spectra in Figure 10a. We have also

seen from the ToF-SIMS depth profile in Figure 8a that the chloride ions are found even in the inner chemisorbed layer on this sample, signifying that the chloride ions have penetrated regions of this organic barrier layer.

For the sample pre-treated with 2-MBI and at the reduced state (Figure 11c), a conversion layer of 2-MBI complexes was already formed upon cathodic polarisation by the release of Cu(I) from the native oxide, thus also forming a bi-layered inhibiting interface but oxide-free and thicker than after pre-treatment without 2-MBI. The formation of complexes was verified by the low intensity of the O 1s spectrum of curve (b) in Figure 4 and the high intensity of the Cu(I) ions in the Cu LMM Auger spectra in Figure 5b. At the reduced state, we already observed the presence of the chloride ions in the inner chemisorbed layer with the complexes suggesting that there are defects in the organic layer, thus rendering the organic layer not as protective as that on the sample pre-treated in absence of 2-MBI.

At the anodic state (Figure 11d), the interface is non-homogeneously attacked, with regions of the un-attacked Cu substrate and regions of the attacked substrate both covered by the organic bilayer, as seen from the ToF-SIMS depth profile in Figure 8b. The ion profile representing the chloride ions exhibits a very high intensity up until the inner copper substrate is reached, as shown in the model. The non-homogeneous attack of the substrate suggests an uneven protection offered by the 2-MBI organic bilayer, with the barrier properties of the inner chemisorbed layer possibly depending on the conversion reactions and local formation of Cu(I)-2-MBI complexes.

## Conclusion

The 2-MBI inhibiting interfaces formed on copper surfaces in an acidic chloride media along with its corrosion protection capabilities of the organic layer were investigated in the present work. The main conclusions are as follows:

- Pre-treatment of the copper surfaces by cathodic reduction in the absence of 2-MBI results in a near oxide free surface, while that in the presence of 2-MBI results in the formation of a conversion layer of Cu(I)-2-MBI metal organic complexes by the consumption of oxygen and release of Cu(I) ions from the native copper oxide film. This was confirmed by the low intensity of oxygen observed from XPS and ToF-SIMS for the sample pre-treated in presence of 2-MBI, but an unusually high intensity for Cu(I) ions from the Cu LMM Auger spectrum.
- The bonding between copper and 2-MBI occurs primarily by the nitrogen atoms of the molecule. For the surface pre-treated in absence of 2-MBI, sulphur bonding to metallic Cu was also observed by XPS analysis.
- Depth profiling by ToF-SIMS revealed the formation of an inner chemisorbed layer and an outer physisorbed layer of the organic 2-MBI film.
- CV corrosion tests confirmed that 2-MBI does protect the metal from corrosive attack, as seen by a positive shift in the potential for the onset of anodic dissolution and a slower increasing anodic current density. However, the protection offered to the metal varied depending on the pre-treatment used.
- For the sample pre-treated in absence of 2-MBI followed by 1 hour exposure to 2-MBI, which exhibited the highest resistance to corrosion initiation, a small anodic peak was observed prior to the initiation of anodic dissolution indicating a side protection reaction. This reaction corresponds to the formation of complexes resulting from the anodic oxidation of Cu metal to Cu(I) ions.
- Upon anodic polarisation, a thicker organic layer was formed on both substrates, seen by both XPS and ToF-SIMS, due to further formation of metal organic complexes.
- On the sample pre-treated with 2-MBI, the top-most substrate surface was non-homogeneously attacked by chloride ions, as evidenced by the shape of the ToF-SIMS depth profiles and the chlorine intensity from XPS analysis. The sample pre-treated in absence of 2-MBI followed by 1 hour exposure to 2-MBI exhibited better protection at the same anodic potential and a much lower chlorine intensity from XPS analysis,

demonstrating that electrochemical control of formation of the interface is instrumental for optimizing the inhibition properties.

## Credit authorship contribution statement

**Vishant Garg**: Investigation, Formal analysis, Writing – original draft, review & editing.

**Sandrine Zanna:** Investigation, Validation, Writing – review & editing.

**Antoine Seyeux:** Investigation, Validation, Writing – review & editing.

**Frédéric Wiame**: Conceptualization, Validation, Writing – review & editing, Supervision.

**Vincent Maurice**: Conceptualization, Validation, Writing – review & editing, Supervision, Funding acquisition.

**Philippe Marcus**: Conceptualization, Writing – review & editing, Supervision, Funding acquisition, Project management.

## Declaration of Competing Interest

The authors declare that they have no known competing financial interests or personal relationships that could have appeared to influence the work reported in this paper.

## Acknowledgements

This project has received funding from the European Research Council (ERC) under the European Union's Horizon 2020 research and innovation program (ERC Advanced grant no. 741123).

Région Ile-de-France is acknowledged for partial funding of the XPS and ToF-SIMS systems.

# References


[1] E. Touzé, C. Cougnon, Study of the air-formed oxide layer at the copper surface and its impact on the copper corrosion in an aggressive chloride medium, Electrochim Acta 262 (2018) 206–213. https://doi.org/10.1016/j.electacta.2017.12.187.

[2] F. King, Corrosion of copper in alkaline chloride environments, Integrity Corrosion Consulting Ltd., Canada, & Swedish Nuclear Fuel and Waste Management Co., Sweden, 2002.

[3] J. Ambrose, R.G. Barradas, D.W. Shoesmith, Investigations of copper in aqueous alkaline solutions by cyclic voltammetry, J Electroanal Chem Interfacial Electrochem 47 (1973) 47–64. https://doi.org/10.1016/S0022-0728(73)80344-4.

[4] B. Miller, Split-Ring Disk Study of the Anodic Processes at a Copper Electrode in Alkaline Solution, J Electrochem Soc 116 (1969) 1675. https://doi.org/10.1149/1.2411657.

[5] W. Kautek, J.G. Gordon, XPS Studies of Anodic Surface Films on Copper Electrodes, J Electrochem Soc 137 (1990) 2672. https://doi.org/10.1149/1.2087008.

[6] M.R. Pinnel, H.G. Tompkins, D.E. Heath, Oxidation of copper in controlled clean air and standard laboratory air at 50°C to 150°C, Applications of Surface Science 2 (1979) 558–577. https://doi.org/10.1016/0378-5963(79)90047-3.

[7] F.K. Crundwell, The Anodic dissolution of copper in hydrochloric acid solutions, Electrochim Acta 31 (1992) 2701–2714. https://doi.org/10.1016/0013-4686(92)85197-S.

[8] G. Kear, B.D. Barker, F.C. Walsh, Electrochemical corrosion of unalloyed copper in chloride media--a critical review, Corros Sci 46 (2004) 109–135. https://doi.org/10.1016/S0010-938X(02)00257-3.

[9] Y. Feng, K.-S. Siow, W.-K. Teo, K.-L. Tan, A.-K. Hsieh, Corrosion Mechanisms and Products of Copper in Aqueous Solutions at Various pH Values, CORROSION 53 (1997). https://doi.org/10.5006/1.3280482.

[10] J.-P. Diard, J.-M. Le Canut, B. Le Gorrec, C. Montella, Copper electrodissolution in 1 M HCl at low current densities. I. General steady-state study, Electrochim Acta 43 (1998) 2469–2483. https://doi.org/10.1016/S0013-4686(97)10155-4.

[11] J.-P. Diard, J.-M. Le Canut, B. Le Gorrec, C. Montella, Copper electrodissolution in 1 M HCl at low current densities. II. Electrochemical impedance spectroscopy study, Electrochim Acta 43 (1998) 2485–2501. https://doi.org/10.1016/S0013-4686(97)10156-6.

[12] J. Turnbull, R. Szukalo, D. Zagidulin, M. Biesinger, D. Shoesmith, The kinetics of copper corrosion in nitric acid, Materials and Corrosion 72 (2021) 348–360. https://doi.org/10.1002/maco.202011707.

[13] M. Pourbaix, Atlas of Electrochemical Equilibria in-Aqueous Solutions, NACE, 1966.

[14] A.G.G. Allah, M.M. Abou-Romia, W.A. Badawy, H.H. Rehan, Effect of halide ions on passivation and pitting corrosion of copper in alkaline solutions, Werkstoffe Und Korrosion 42 (1991) 584–591. https://doi.org/10.1002/maco.19910421105.

[15] K. Rokosz, T. Hryniewicz, D. Matỳsek, S. Raaen, J. Valíček, Ł. Dudek, M. Harničárová, SEM, EDS and XPS analysis of the coatings obtained on titanium after plasma electrolytic oxidation in electrolytes containing copper nitrate, Materials 9 (2016). https://doi.org/10.3390/ma9050318.

[16] H. Parangusan, J. Bhadra, N. Al-Thani, A review of passivity breakdown on metal surfaces: influence of chloride- and sulfide-ion concentrations, temperature, and pH, Emergent Mater 4 (2021) 1187–1203. https://doi.org/10.1007/s42247-021-00194-6.

[17] V. Brusic, M.A. Frisch, B.N. Eldridge, F.P. Novak, F.B. Kaufman, B.M. Rush, G.S. Frankel, Copper Corrosion With and Without Inhibitors, J Electrochem Soc 138 (1991) 2253. https://doi.org/10.1149/1.2085957.

[18] A. Shaban, E. Kálmán, J. Telegdi, G. Pálinkás, G. Dóra, Corrosion and inhibition of copper in different electrolyte solutions, Applied Physics A 66 (1998) 545–549. https://doi.org/10.1007/s003390051199.

[19] M.B.P. Mihajlović, M.M. Antonijević, Copper Corrosion Inhibitors. Period 2008-2014. A Review, Int J Electrochem Sci 10 (2015) 1027–1053. https://doi.org/10.1016/S1452-3981(23)05053-8.

[20] A. Fateh, M. Aliofkhazraei, A.R. Rezvanian, Review of corrosive environments for copper and its corrosion inhibitors, Arabian Journal of Chemistry 13 (2020) 481–544. https://doi.org/10.1016/j.arabjc.2017.05.021.

[21] X. Wu, F. Wiame, V. Maurice, P. Marcus, Molecular scale insights into interaction mechanisms between organic inhibitor film and copper, Npj Mater Degrad 5 (2021). https://doi.org/10.1038/s41529-021-00168-3.

[22] X. Wu, F. Wiame, V. Maurice, P. Marcus, 2-Mercaptobenzimidazole films formed at ultra-low pressure on copper: adsorption, thermal stability and corrosion inhibition performance, Appl Surf Sci 527 (2020). https://doi.org/10.1016/j.apsusc.2020.146814.

[23] S.B. Sharma, V. Maurice, L.H. Klein, P. Marcus, In situ scanning tunneling microscopy study of 2-mercaptobenzimidazole local inhibition effects on copper corrosion at grain boundary surface terminations, Electrochim Acta 378 (2021). https://doi.org/10.1016/j.electacta.2021.138150.

[24] M. Finšgar, 2-Mercaptobenzimidazole as a copper corrosion inhibitor: Part I. Long-term immersion, 3D-profilometry, and electrochemistry, Corros Sci 72 (2013) 82–89. https://doi.org/10.1016/j.corsci.2013.03.011.

[25] D.K. Kozlica, J. Izquierdo, R.M. Souto, I. Milošev, Inhibition of the localised corrosion of AA2024 in chloride solution by 2-mercaptobenzimidazole and octylphosphonic acid, Npj Mater Degrad 7 (2023). https://doi.org/10.1038/s41529-023-00368-z.

[26] M.R. Jakeria, L. Ward, I. Cole, Long term durability studies on the corrosion inhibition effect of 2-mercaptobenzimidazole (C3H4N2S) on AA6022: Mechanism of film formation and influence of IMPs, Surfaces and Interfaces 25 (2021). https://doi.org/10.1016/j.surfin.2021.101164.

[27] G. Žerjav, I. Milošev, Corrosion protection of brasses and zinc in simulated urban rain: Part I: Individual inhibitors benzotriazole, 2-mercaptobenzimidazole and stearic acid, Materials and Corrosion 66 (2015) 1402–1413. https://doi.org/10.1002/maco.201508383.

[28] M. Mahdavian, S. Ashhari, Corrosion inhibition performance of 2-mercaptobenzimidazole and 2-mercaptobenzoxazole compounds for protection of mild steel in hydrochloric acid solution, Electrochim Acta 55 (2010) 1720–1724. https://doi.org/10.1016/j.electacta.2009.10.055.

[29] S.A.M. Refaey, F. Taha, A.M. Abd El-Malak, Corrosion and Inhibition of 316L stainless steel in neutral medium by 2-Mercaptobenzimidazole, Int J Electrochem Sci 1 (2006) 80–91. https://doi.org/10.1016/S1452-3981(23)17138-0.

[30] B. Assouli, A. Srhiri, H. Idrissi, Effect of 2-Mercaptobenzimidazole and Its Polymeric Film on the Corrosion Inhibition of Brass (60/40) in Ammonia Solution, CORROSION 60 (2004) 399–407. https://doi.org/10.5006/1.3287749.

[31] L. Wang, J.-X. Pu, H.-C. Luo, Corrosion inhibition of zinc in phosphoric acid solution by 2-mercaptobenzimidazole, Corros Sci 45 (2003) 677–683. https://doi.org/doi.org/10.1016/S0010-938X(02)00145-2.

[32] G.R. Form, E.S. Raper, T.C. Downie, The crystal and molecular structure of 2-mercaptobenzimidazole, Acta Crystallogr B 32 (1976) 345–348. https://doi.org/10.1107/s0567740876003026.

[33] S.M. Ansar, R. Haputhanthri, B. Edmonds, D. Liu, L. Yu, A. Sygula, D. Zhang, Determination of the binding affinity, packing, and conformation of thiolate and thione ligands on gold nanoparticles, Journal of Physical Chemistry C 115 (2011) 653–660. https://doi.org/10.1021/jp110240y.

[34] F.X. Perrin, J. Pagetti, Characterization and mechanism of direct film formation on a Cu electrode through electro-oxidation of 2-mercaptobenzimidazole, Corros Sci 40 (1998) 1647–1662. https://doi.org/10.1016/S0010-938X(98)00060-2.

[35] M. Finšgar, 2-Mercaptobenzimidazole as a copper corrosion inhibitor: Part II. Surface analysis using X-ray photoelectron spectroscopy, Corros Sci 72 (2013) 90–98. https://doi.org/10.1016/j.corsci.2013.03.010.

[36] R. Subramanian, V. Lakshminarayanan, Effect of adsorption of some azoles on copper passivation in alkaline medium, Corros Sci 44 (2002) 535–554. https://doi.org/10.1016/S0010-938X(01)00085-3.

[37] F. Chiter, D. Costa, V. Maurice, P. Marcus, Atomic Scale Insight into Corrosion Inhibition: DFT Study of 2-Mercaptobenzimidazole on Locally De-Passivated Copper Surfaces, J Electrochem Soc 168 (2021) 121507. https://doi.org/10.1149/1945-7111/ac405c.

[38] F. Chiter, D. Costa, V. Maurice, P. Marcus, Adsorption of 2-mercaptobenzimidazole Corrosion Inhibitor on Copper: DFT Study on Model Oxidized Interfaces, J Electrochem Soc 167 (2020) 161506. https://doi.org/10.1149/1945-7111/abcd4f.

[39] D.Q. Zhang, L.X. Gao, G.D. Zhou, Inhibition of copper corrosion in aerated hydrochloric acid solution by heterocyclic compounds containing a mercapto group, Corros Sci 46 (2004) 3031–3040. https://doi.org/10.1016/j.corsci.2004.04.012.

[40] D. Chadwick, T. Hashemi, Electron spectroscopy of corrosion inhibitors: Surface films formed by 2-mercaptobenzothiazole and 2-mercaptobenzimidazole on copper., Surf Sci 89 (1979) 649–659. https://doi.org/10.1016/0039-6028(79)90646-0.

[41] G. Xue, X.-Y. Huang, J. Dong, J. Zhang, The formation of an effective anti-corrosion film on copper surfaces from 2-mercaptobenzimidazole solution, J Electroanal Chem Interfacial Electrochem 310 (1991) 139–148. https://doi.org/10.1016/0022-0728(91)85257-P.

[42] E. Martinez-Lombardia, V. Maurice, L. Lapeire, I. De Graeve, K. Verbeken, L. Kestens, P. Marcus, H. Terryn, In situ scanning tunneling microscopy study of grain-dependent corrosion on microcrystalline copper, Journal of Physical Chemistry C 118 (2014) 25421–25428. https://doi.org/10.1021/jp507089f.

[43] V. Garg, S.B. Sharma, S. Zanna, A. Seyeux, F. Wiame, V. Maurice, P. Marcus, Enhanced corrosion inhibition of copper in acidic environment by cathodic control of interface formation with 2-mercaptobenzothiazole, Electrochim Acta 447 (2023) 142162. https://doi.org/10.1016/j.electacta.2023.142162.

[44] V. Garg, S. Zanna, A. Seyeux, F. Wiame, V. Maurice, P. Marcus, Adsorption of 2-Mercaptobenzothiazole Organic Inhibitor and its Effects on Copper Anodic Oxidation in Alkaline Environment, J Electrochem Soc 170 (2023) 071502. https://doi.org/10.1149/1945-7111/ace33b.

[45] V. Garg, S. Zanna, A. Seyeux, F. Wiame, V. Maurice, P. Marcus, Inhibition of the initial stages of corrosion by 2-mercaptobenzothiazole adsorption and the effects of interfacial oxides on copper in neutral chloride conditions, Corros Sci 225 (2023) 111596. https://doi.org/10.1016/j.corsci.2023.111596.

[46] S. Mirhashemihaghighi, J. Światowska, V. Maurice, A. Seyeux, L.H. Klein, E. Härkönen, M. Ritala, P. Marcus, Electrochemical and Surface Analysis of the Corrosion Protection of Copper by Nanometer-Thick Alumina Coatings Prepared by Atomic Layer Deposition, J Electrochem Soc 162 (2015) C377–C384. https://doi.org/10.1149/2.0081508jes.

[47] J.H. Scofield, Hartree-Slater Subshell Photoionization cross-sections at 1254 and 1487 eV, J Electron Spectros Relat Phenomena 8 (1976) 129–137. https://doi.org/10.1016/0368-2048(76)80015-1.

[48] H. Shinotsuka, S. Tanuma, C.J. Powell, Calculations of electron inelastic mean free paths. XIII. Data for 14 organic compounds and water over the 50 eV to 200 keV range with the relativistic full Penn algorithm, Surface and Interface Analysis 54 (2022) 534–560. https://doi.org/10.1002/sia.7064.

[49] J.W. Diggle, T.C. Downie, C.W. Goulding, Anodic Oxide Films On Aluminum, Chem Rev 69 (1969) 365–405. https://doi.org/10.1021/cr60259a005.

[50] X. Wu, F. Wiame, V. Maurice, P. Marcus, 2-Mercaptobenzothiazole corrosion inhibitor deposited at ultra-low pressure on model copper surfaces, Corros Sci 166 (2020) 108464. https://doi.org/10.1016/j.corsci.2020.108464.

[51] X. Wu, F. Wiame, V. Maurice, P. Marcus, Effects of water vapour on 2-mercaptobenzothiazole corrosion inhibitor films deposited on copper, Corros Sci 189 (2021) 109565. https://doi.org/10.1016/j.corsci.2021.109565.

[52] X. Wu, F. Wiame, V. Maurice, P. Marcus, Moiré Structure of the 2-Mercaptobenzothiazole Corrosion Inhibitor Adsorbed on a (111)-Oriented Copper Surface, Journal of Physical Chemistry C 124 (2020) 15995–16001. https://doi.org/10.1021/acs.jpcc.0c04083.

[53] J.F. Moulder, W.F. Stickle, P.E. Sobol, K.D. Bomben, J. Chastain, Handbook of X-ray Photoelectron Spectroscopy: A Reference Book of Standard Spectra for Identification and Interpretation of XPS Data, PerkinElmer Corporation, Eden Prairie, Minnesota, 1992.

[54] A. Galtayries, J.P. Bonnelle, XPS and ISS studies on the interaction of H2S with polycrystalline Cu, Cu2O and CuO surfaces, Surface and Interface Analysis 23 (1995) 171–179. https://doi.org/10.1002/sia.740230308.

[55] C.M. Whelan, M.R. Smyth, C.J. Barnes, N.M.D. Brown, C.A. Anderson, An XPS study of heterocyclic thiol self-assembly on Au 111, Appl Surf Sci 134 (1998) 144–158.

[56] A. Seyeux, S. Zanna, A. Allion, P. Marcus, The fate of the protective oxide film on stainless steel upon early stage growth of a biofilm, Corros Sci 91 (2015) 352–356. https://doi.org/10.1016/j.corsci.2014.10.051.